

Average-atom approach for transport properties of shocked argon in the presence of a magnetic field

Nadine Wetta ^{1,*} and Jean-Christophe Pain ^{1,2}

¹*CEA, DAM, DIF, F-91297 Arpajon, France*

²*Université Paris-Saclay, CEA, Laboratoire Matière en Conditions Extrêmes, 91680 Bruyères-le-Châtel, France*



(Received 7 May 2024; accepted 12 June 2024; published 2 July 2024)

We present electron transport calculations of shocked argon based on an average-atom modeling of the plasma and compare them with measurements, involving both incident and reflected shock waves. Since the corresponding experiments are subject to a 5 T magnetic field, the impact of the latter on the Rankine-Hugoniot equations is taken into account, starting from the magnetoresistive hydrodynamics, and the resistivity tensor is deduced from the Boltzmann equation. The resistivity tensor yields the electrical and Hall resistivities. Our average-atom code PARADISIO provides the quantities required for the calculation of electrical resistivity within the Ziman-Evans formalism, as well as for the Hall resistivity. We obtain good agreement between calculated conductivities and experimental values, both for the incident and reflected shocks. Our values of the Hall constant are compared to experimental values derived from Hall voltage measurements, as well as to theoretical ones based on the quantum statistical linear-relaxation-time approach.

DOI: [10.1103/PhysRevE.110.015202](https://doi.org/10.1103/PhysRevE.110.015202)

I. INTRODUCTION

Argon is the most abundant noble gas on Earth, and is also present in the atmosphere of gaseous giant planets [1–3]. Understanding the physics of the latter requires accurate equations of state (EOS), as well as theoretical transport coefficients for this element. More generally, argon is also an ideal candidate for theoretical studies of warm dense matter (WDM), due to its high ionization energy (15.76 eV [4], only surpassed by He, F, and Ne). As a result, argon remains in partially ionized states over wide density and temperature ranges. Partial ionization is one of the main features of WDM, and the determination of the free-electron density n_e is of particular importance under these conditions. Experiments are also essential as reference points for WDM theoretical models.

Experiments involving noble gas plasmas, including He, Ne, Ar, Kr, and Xe, have been conducted over the last 30 years using explosively driven shock wave plasmas. Noble gas plasmas were created with temperatures T of 6000–10⁵ K and densities of 0.001–10 g/cm³ [5–7]. The direct current (dc) conductivity was measured in each experiment. In the most recent experiments by Shilkin *et al.* [7], shock-loading experiments have been realized in the presence of magnetic fields for Xe and Ar, providing measurements of the Hall voltage. The latter are expected to be a more direct diagnostic tool for n_e than electrical conductivity.

To properly describe transport properties of dense plasmas, a consistent quantum statistical description of electronic structure is necessary. Adams *et al.* used an approach based on linear response theory (LRT) as proposed by Zubarev [8,9], to

describe transport properties in terms of force-force correlation functions calculated within perturbation theory [10–13]. This model enables a complete description of partially ionized plasmas, accounting for electron interactions with other electrons, with different ionic species (carrying different charges $Z = 1, 2, \dots$) and with neutral argon atoms. To the best of our knowledge, to date their work represents the most complete theoretical study of the transport properties in argon under these very weak ionization conditions.

In this paper, we present an alternative study based on the use of the average-atom method to derive a collision frequency between electrons and a mean ion, whose low charge is representative of the average charge carried by the actual various ion species. This approach avoids the difficulties of calculating the actual plasma composition and of modeling different collision frequencies between electrons and numerous species composing the plasma. Electron-ion collisions are easily obtained with the T -matrix formalism. As far as we know, there are few theoretical models for the electron-neutral collision frequency under the conditions reached in the experiments carried out by Shilkin *et al.* on argon.

Average-atom models are commonly used for dc electrical resistivity calculations within the Ziman-Evans formalism (see, for instance, Refs. [14–19]), which was extended to other electron-transfer coefficients for the fully ionized, fully degenerate hydrogen plasma [20].

The main features of Ziman’s formalism for conductivity are recalled in Sec. II, as well as the way the required quantities are derived from our average-atom code PARADISIO, also described within this section.

Section III opens with a brief description of the shock-loading experiments of Shilkin *et al.* on argon. Starting from the magnetohydrodynamics equations, the Rankine-Hugoniot relations in presence of a magnetic field are derived.

*Contact author: nadine.wetta@cea.fr

The Rankine-Hugoniot equations relate the thermodynamical conditions behind the shock wave to the incident ones. In the presence of an external magnetic field, the relation between an applied electric field and the induced electric current is tensorial. We recall the main steps leading to the resistivity tensor, starting from the Boltzmann equation.

Section IV presents our numerical electrical conductivity and Hall resistivity calculations in the conditions of the experiments of Shilkin *et al.* Our results are compared to experimental values and, concerning Hall effect, to other theoretical results.

In Sec. V, we focus on comparisons with the LRT Hall constant calculations of Adams *et al.* The relevance of average-atom methods for these calculations in partially ionized plasmas is discussed, before finally concluding this paper by a brief summary (Sec. VI).

II. CALCULATION OF ELECTRICAL RESISTIVITY IN THE FRAMEWORK OF THE AVERAGE-ATOM MODEL

A. The Ziman-Evans formulation

The Ziman resistivity formula [21] reads

$$\eta = -\frac{1}{3\pi Z^* n_i} \frac{\hbar}{e^2} \int_0^\infty \frac{\partial f}{\partial \epsilon}(\epsilon, \mu^*) \mathcal{I}(\epsilon) d\epsilon, \quad (2.1)$$

where n_i is the ion density, Z^* the mean ionic charge, μ^* the chemical potential. $f(\epsilon, \mu^*)$ is the Fermi-Dirac distribution function,

$$f(\epsilon, \mu^*) = \frac{1}{1 + e^{\beta(\epsilon - \mu^*)}}, \quad (2.2)$$

where $\beta = 1/(k_B T)$, k_B denoting the Boltzmann constant. To be consistent with the uniform electron gas (UEG) assumption underlying the Ziman theory, the chemical potential μ^* is given by

$$Z^* n_i = \frac{\sqrt{2}}{\pi^2 \beta^{3/2}} \mathcal{F}_{1/2}(\beta \mu^*), \quad (2.3)$$

where

$$\mathcal{F}_{1/2}(x) = \int_0^\infty dt \frac{t^{1/2}}{e^{t-x} + 1} \quad (2.4)$$

defines the Fermi function of order 1/2. The function $\mathcal{I}(\epsilon)$ is related to the scattering cross-section $\Sigma(q)$ and to the ion-ion structure factor $S(q)$ by

$$\mathcal{I}(\epsilon) = \int_0^{2k} q^3 S(q) \Sigma(q) dq, \quad (2.5)$$

where $\vec{q} = \vec{k}' - \vec{k}$ is the momentum transferred in the elastic scattering event, (i.e., in which $|\vec{k}'| = |\vec{k}|$). Introducing the scattering angle $\theta \equiv (\vec{k}, \vec{k}')$, one has $q^2 = 2k^2(1 - \chi)$, where $\chi = \cos\theta$, and one gets then the following expression introducing the squared modulus of the scattering amplitude $|a(k, \chi)|^2$:

$$\mathcal{I}(\epsilon) = 2k^4 \int_{-1}^1 S[k\sqrt{2(1-\chi)}] |a(k, \chi)|^2 (1-\chi) d\chi. \quad (2.6)$$

$|a(k, \chi)|^2$ is provided by the T -matrix formalism of Evans [22] which reads, in the relativistic formalism underlying our

average-atom code PARADISIO [15,23],

$$|a(k, \chi)|^2 = \frac{1}{k^2} \left(\left| \sum_{\kappa} |\kappa| e^{i\delta_{\kappa}(k)} \sin[\delta_{\kappa}(k)] P_{\ell}(\chi) \right|^2 + \left| \sum_{\kappa} \frac{|\kappa|}{i\kappa} e^{i\delta_{\kappa}(k)} \sin[\delta_{\kappa}(k)] P_{\ell}^1(\chi) \right|^2 \right), \quad (2.7)$$

where $\kappa = -(\ell + 1)$ for $j = \ell + 1/2$, $\kappa = \ell$ for $j = \ell - 1/2$, ℓ being the usual orbital quantum number. P_{ℓ} and P_{ℓ}^1 are the Legendre and associated Legendre polynomials. Finally, the quantities $\delta_{\kappa}(k)$ denote the scattering phase-shifts.

In the present paper, the mean ionic charge Z^* and the scattering phase-shifts $\delta_{\kappa}(k)$ are provided by the average-atom code PARADISIO. Outputs from this code are also used to build the ion-ion structure factor $S(q)$.

B. The average-atom model PARADISIO

Atomic units where $e = \hbar = m_e = 1$, and where the velocity of light $c = 137.036$ is the inverse of the fine structure constant $\alpha = e^2/(8\pi\epsilon_0 a_B)$, a_B being the Bohr radius and ϵ_0 the permittivity of vacuum, are used throughout this section.

The PARADISIO [23] code is based on Liberman's relativistic quantum-average-atom model INFERNO [24], which considers the atom as a point nucleus surrounded by its Z electrons, placed at the center of a spherical cavity of radius R_{ws} dug into a jellium. The Wigner-Seitz radius R_{ws} reads

$$R_{ws} = \left(\frac{3}{4\pi} \frac{A/\mathcal{N}_{Avo}}{\rho} \right)^{1/3}, \quad (2.8)$$

with ρ , A , and \mathcal{N}_{Avo} denoting, respectively, the mass density, molar mass and Avogadro number.

The jellium consists of a uniform electron gas and a uniform distribution of positive charges that ensures its electrical neutrality. The INFERNO model also imposes electrical neutrality inside the cavity. The electronic structure is computed in a self-consistent way. The only required parameters are atomic number Z , molar mass A , mass density ρ , and temperature T .

In this spherical symmetry, the one-electron wave functions, solutions of the Dirac equation, are of the form

$$\psi_s(\vec{r}) \equiv \psi_{j\ell m}(\vec{r}) = \begin{pmatrix} \frac{1}{r} F(r) \Omega_{j\ell m}(\theta, \phi) \\ -\frac{i}{r} G(r) \Omega_{j\ell' m}(\theta, \phi) \end{pmatrix}, \quad (2.9)$$

where $\Omega_{j\ell m}$ and $\Omega_{j\ell' m}$ are two spinors. j , ℓ , and m are quantum numbers associated, respectively, to the total angular momentum J , to the orbital angular momentum L , and its projection L_z on the z axis. The quantum number ℓ' is given by

$$\ell' = \begin{cases} \ell + 1 & \text{if } j = \ell + 1/2 \\ \ell - 1 & \text{if } j = \ell - 1/2. \end{cases} \quad (2.10)$$

The Dirac equation then reduces to the following equations satisfied by the radial functions $F(r)$ and $G(r)$:

$$\begin{cases} \frac{dF}{dr} = -\frac{\kappa}{r} F(r) - \frac{V_{\text{eff}}(r) - c^2 - \epsilon}{c} G(r) \\ \frac{dG}{dr} = \frac{V_{\text{eff}}(r) + c^2 - \epsilon}{c} F(r) + \frac{\kappa}{r} G(r), \end{cases} \quad (2.11)$$

where

$$\begin{cases} \kappa = -(\ell + 1) & \text{for } j = \ell + 1/2 \\ \kappa = \ell & \text{for } j = \ell - 1/2. \end{cases} \quad (2.12)$$

Outside the cavity, the effective potential $V_{\text{eff}}(r)$ is constant and given by

$$V_{\infty} = \mu_{\text{xc}}[\bar{n}, T], \quad (2.13)$$

with \bar{n} denoting the density of the jellium.

$$\bar{n} = \frac{\sqrt{2}}{\pi^2 \beta^{3/2}} \mathcal{F}_{1/2}(\beta\mu), \quad (2.14)$$

with the Fermi function $\mathcal{F}_{1/2}(\beta\mu)$ expression given in Eq. (2.4). $\mu_{\text{xc}}[\bar{n}, T]$ is the electron exchange-correlation potential functional evaluated at the UEG density \bar{n} and at temperature T . PARADISIO uses the finite temperature functionals of the KSDT form [25] with revised parameters from Groth *et al.* [26].

The model imposes $F(r) = G(r) = 0$ at $r = 0$ and $r \rightarrow \infty$. Outside the cavity, the radial functions $F^{\text{oc}}(r)$ and $G^{\text{oc}}(r)$ (the superscript oc stands for outside cavity) satisfying those boundary conditions are, for bound states (i.e., for energies $\epsilon < V_{\infty}$), modified Bessel functions of the third kind [27], exponentially decreasing,

$$\epsilon < V_{\infty} : \begin{cases} F_{\text{b}}^{\text{oc}}(r) = a_0 \frac{kc}{\epsilon - V_{\infty}} r K_{\ell+1/2}(kr) \\ G_{\text{b}}^{\text{oc}}(r) = a_0 r K_{\ell+1/2}(kr), \end{cases} \quad (2.15)$$

and, for free states, (i.e., for energies $\epsilon \geq V_{\infty}$), combinations of Bessel functions of the first and second kinds, with decreasing amplitudes as $r \rightarrow \infty$,

$$\epsilon \geq V_{\infty} : \begin{cases} F_{\text{f}}^{\text{oc}}(r) = b_0 \frac{kc}{\epsilon - V_{\infty}} r [\cos(\delta_{\kappa}) j_{\ell}(kr) - \sin(\delta_{\kappa}) n_{\ell}(kr)] \\ G_{\text{f}}^{\text{oc}}(r) = b_0 r [\cos(\delta_{\kappa}) j_{\ell'}(kr) - \sin(\delta_{\kappa}) n_{\ell'}(kr)], \end{cases} \quad (2.16)$$

where a_0 and b_0 are two normalization factors. PARADISIO then only needs to solve Eq. (2.11) inside the cavity. The continuity condition at the cavity radius $r = R_{\text{ws}}$ is only possible for discrete values of the energies $\epsilon < V_{\infty}$, yielding the bound states. The matching of inside and outside solutions is possible at any energy $\epsilon \geq V_{\infty}$ by adjusting the phase shifts $\delta_{\kappa}(k)$, giving the continuum of free states.

The electronic density $n(r)$ is then obtained by

$$\begin{aligned} n(r) &= \sum_{\text{b}} \sum_{\kappa} 2|\kappa| [F_{\text{b}}(r, \kappa, \epsilon_{\text{b}})^2 + G_{\text{b}}(r, \kappa, \epsilon_{\text{b}})^2] \\ &+ \int_0^{\infty} d\epsilon \sum_{\kappa} 2|\kappa| [F_{\text{f}}(r, \kappa, \epsilon)^2 + G_{\text{f}}(r, \kappa, \epsilon)^2]. \end{aligned} \quad (2.17)$$

The number Z_{bound} of bound electrons and the number Z_{cont} of continuum ones, respectively, read

$$\begin{aligned} Z_{\text{bound}} &= \sum_{\text{b}} f(\epsilon_{\text{b}}, \mu) \sum_{\kappa} 2|\kappa| \\ &\times \left\{ \int_0^{R_{\text{ws}}} [F_{\text{b}}(r, \kappa, \epsilon_{\text{b}})^2 + G_{\text{b}}(r, \kappa, \epsilon_{\text{b}})^2] r^2 dr \right\} \end{aligned} \quad (2.18)$$

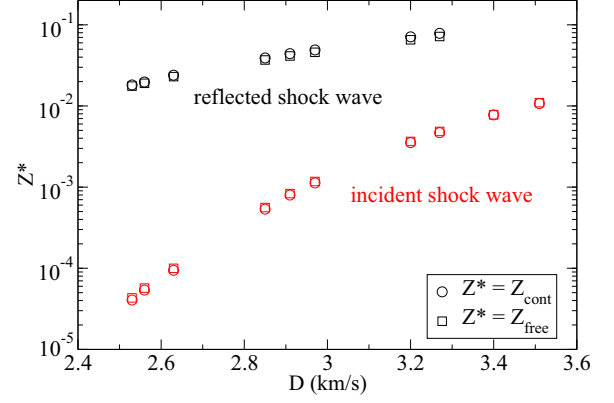


FIG. 1. Argon mean ion charge Z^* in the conditions of the shock experiments of Shilkin *et al.* from our average-atom code, using two widely used definitions. $Z^* = Z_{\text{cont}}$, is the one based on the continuum density of states, giving the values represented by the circles. The squares correspond to $Z^* = Z_{\text{free}}$, i.e., the number deduced from the jellium's density of states. The data relative to the incident shock waves are presented in red, and those corresponding to the reflected shocks in black. D denotes the shock speeds.

and

$$\begin{aligned} Z_{\text{cont}} &= \int_0^{\infty} d\epsilon f(\epsilon, \mu) \sum_{\kappa} 2|\kappa| \\ &\times \left\{ \int_0^{R_{\text{ws}}} [F_{\text{f}}(r, \kappa, \epsilon)^2 + G_{\text{f}}(r, \kappa, \epsilon)^2] r^2 dr \right\}. \end{aligned} \quad (2.19)$$

The chemical potential μ is obtained from the charge neutrality condition $Z = Z_{\text{bound}} + Z_{\text{cont}}$ inside the cavity.

C. Mean ionic charge and ion-ion structure factor from the code

The scattering phase shifts $\delta_{\kappa}(k)$ needed by the Ziman formalism are obtained from the continuity condition on the radial functions solutions of Eqs. (2.11) at the cavity radius $r = R_{\text{ws}}$ for $\epsilon \geq V_{\infty}$.

The formalism requires a value for the mean ionic charge Z^* . In the framework of our average-atom approach, the use of Z_{cont} , given by Eq. (2.19) for this quantity seems obvious, as does that of the one obtained from the jellium's charge density, denoted Z_{free} and reading

$$Z_{\text{free}} = \bar{n} \times \left(\frac{4\pi}{3} R_{\text{ws}}^3 \right). \quad (2.20)$$

The value of the chemical potential μ^* required by the Ziman formula is related to the value of Z^* by Eq. (2.3).

In most situations, in particular, when the continuum of energies is uniform electron-gas-like, the two values are close and the impact of their difference on the Ziman resistivity is limited, due to compensation by the chemical potential [28]. In the case of argon in the thermodynamic conditions investigated in the present paper, we found that $Z_{\text{cont}} \approx Z_{\text{free}}$ within a few percents (see Fig. 1). We also did not find quasisubbound or quasi-free-states which would justify corrections of Z_{cont} as recommended in our previous work on low density

metallic plasmas where such states occur [19]. All our resistivity calculations were therefore performed with $Z^* = Z_{\text{cont}}$.

Electrical resistivity calculations within the Ziman approach are sensitive to the ion-ion structure factor $S(q)$ mainly in the WDM conditions. In a study on aluminum at solid density and temperatures ranging from ambient one up to 100 eV, we showed the importance of equivalent modeling of $S(q)$ in the liquid and solid states [18]. Sophisticated models are of less importance in hot plasmas, as well as in low density ones [28]. In the present paper on argon, in which electronic densities remain very small (ranging from 10^{15} up to 10^{19} cm^{-3}), we solve the Ornstein-Zernike equation together with the hypernetted-chain closure relation for a system of screened charged spheres [29].

III. SHOCK-LOADING EXPERIMENTS IN PRESENCE OF A MAGNETIC FIELD

A. Description of Shilkin *et al.*'s experiments [7]

To simplify, the experimental device consists of an approximately 30-cm-long cylinder with an inner diameter of 5 cm, in which an explosive charge is placed in the first 12 up to 15 cm, and the studied gas in the remaining space. Shock waves are formed by the expansion of the detonation products in the gas. It has been checked, by a series of separate experiments, that the shock is one-dimensional and stationary at a distance of 5 up to 10 cm from the end of the charge, which allows for a uniform plasma bunch of several centimeters thick, sufficient for placing probe diagnostics. An obstacle closes the cylinder, enabling shock reflection and further compression and heating of the studied gas. A solenoid is also wound around the cylinder, generating a magnetic field $B = 5 \text{ T}$ along the cylinder axis.

Diagnostic probes provide experimental shock velocities D , electric resistance to an external electric current, and Hall voltage induced by the applied magnetic field. Hall voltage $\mathcal{U}_{\text{Hall}}$ is related to the Hall coefficient R_{Hall} by

$$R_{\text{Hall}} = \frac{h \mathcal{U}_{\text{Hall}}}{Q I B}, \quad (3.1)$$

where I denotes the external electric current, h the plasma thickness, and Q a geometric factor specific to the experimental device and determined in a series of separate experiments. The Hall coefficient varies inversely to the electron density. The latter may therefore be inferred from the Hall voltage measurements.

B. Rankine-Hugoniot relations in absence of a magnetic field

1. Incident shock wave

In the following, the upstream (i.e., before the shock front) thermodynamic conditions are denoted ρ_0 , T_0 , u_0 , and P_0 , respectively, being mass density, temperature, mass internal energy, and pressure. V_0 corresponds to upstream mass velocity and D to shock velocity. Downstream (i.e., beyond the shock wave) thermodynamic conditions are ρ_H , T_H , u_H , and P_H , and the mass velocity V_H (see Fig. 2). The Rankine-Hugoniot jump conditions across a planar shock front consist of three conservation relations. In the reference frame fixed to

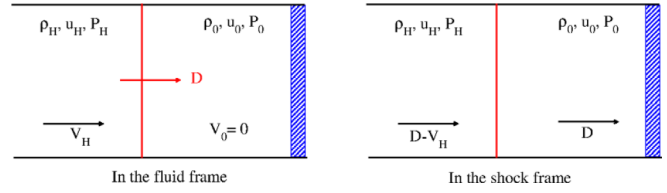


FIG. 2. First shock wave, before reflection on the obstacle, represented in blue. Left: Description in the fluid frame, where the upstream fluid velocity is $V_0 = 0$. Right: Description in the shock frame, where the shock velocity is zero.

the shock,

$$\rho_H(D - V_H) = \rho_0(D - V_0) \quad (3.2)$$

is the first relation, expressing the mass conservation across the shock front,

$$\rho_H(D - V_H)^2 + P_H = \rho_0(D - V_0)^2 + P_0 \quad (3.3)$$

is the momentum conservation law, and

$$\frac{1}{2}(D - V_H)^2 + u_H + \frac{P_H}{\rho_H} = \frac{1}{2}(D - V_0)^2 + u_0 + \frac{P_0}{\rho_0} \quad (3.4)$$

the energy conservation equation. Inserting Eq. (3.2) into Eq. (3.3) yields

$$(D - V_0) = \left[\frac{\rho_H (P_H - P_0)}{\rho_0 (\rho_H - \rho_0)} \right]^{1/2}. \quad (3.5)$$

Using this in Eq. (3.2) gives

$$(V_H - V_0) = (D - V_0) \left(1 - \frac{\rho_0}{\rho_H} \right), \quad (3.6)$$

and putting Eq. (3.5) in Eq. (3.4):

$$(u_H - u_0) + \frac{1}{2}(P_H + P_0) \left(\frac{1}{\rho_H} - \frac{1}{\rho_0} \right) = 0. \quad (3.7)$$

The latter equation, together with an equation of state $u(\rho, T)$ and $P(\rho, T)$, and under the condition that Eq. (3.5) is satisfied, yields the thermodynamic conditions ρ_H , T_H , u_H , and P_H beyond the shock wave, and the value of the downstream velocity V_H as functions of the shock velocity D .

2. Reflected shock wave

In Shilkin *et al.*'s experiments, the shock wave encounters an obstacle, creating a reflected shock wave opposing the shocked plasma moving at velocity V_H (see Fig. 3). The upstream conditions here correspond to the preceding downstream one, i.e., we have $\rho_0 = \rho_H$, $T_0 = T_H$, $u_0 = u_H$, $P_0 = P_H$, and $V_0 = V_H$. In the fluid frame, the reflected shock velocity is $(-D + V_H)$ (Fig. 3, left). We will here denote the downstream quantities ρ , T , u , P , and V . Assuming that the incident shock wave reflects perfectly on the obstacle, the downstream velocity is $V = -V_H + V_H = 0$. Rankine-Hugoniot relations then read, in the shock frame (Fig. 3 right),

$$\rho(D - V_H) = \rho_H D, \quad (3.8)$$

$$\rho(D - V_H)^2 + P = \rho_H D^2 + P_H, \quad (3.9)$$

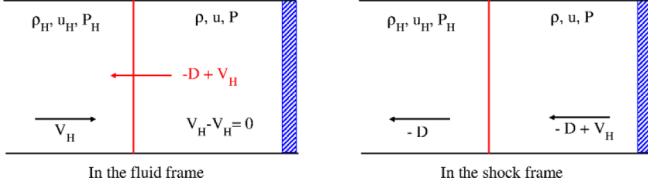


FIG. 3. Second shock wave, after reflection on the obstacle, represented in blue. Left: Description in the fluid frame, where the upstream fluid velocity is $V_0 = -V_H$ and the shock velocity $-D + V_H$, V_H is the fluid velocity downstream the incident shock. Right: Description in the shock frame, where the shock velocity is zero.

and

$$\frac{1}{2}(D - V_H)^2 + u + \frac{P}{\rho} = \frac{1}{2}D^2 + u_H + \frac{P_H}{\rho_H}. \quad (3.10)$$

After performing the same operations as for the incident shock wave case, we get

$$(u - u_H) + \frac{1}{2}(P + P_H) \left(\frac{1}{\rho} - \frac{1}{\rho_H} \right) = 0, \quad (3.11)$$

which, together with our EOS $u(\rho, T)$ and $P(\rho, T)$, and under the constraint that

$$V_H = \left(1 - \frac{\rho_H}{\rho} \right) \left[\frac{\rho}{\rho_H} \frac{(P - P_H)}{(\rho - \rho_H)} \right]^{1/2}, \quad (3.12)$$

yields the thermodynamic conditions ρ , T , u , and P beyond the reflected shock wave, as functions of the upstream mass velocity V_H reach the incident shock downstream.

C. Impact of the external magnetic field on Rankine-Hugoniot relations

Up to now, we did not take into account the existence of the magnetic field present in Shilkin *et al.*'s experiments for the need for Hall effect measurements. The magnetic field interacts strongly with the plasma flow, and the Rankine-Hugoniot relations must be revised within the framework of magnetohydrodynamic theory.

The flow of a compressible, nonviscous heat-insulating fluid in a magnetic field is described by a set of continuity relations [30], commonly referred to as Euler's equations, coupled to Maxwell's relations. The first Euler equation expresses the conservation of mass:

$$\frac{\partial \rho}{\partial t} + \vec{\nabla} \cdot (\rho \vec{V}) = 0. \quad (3.13)$$

The second relation is the actual Euler's equation [31], and expresses the conservation of momentum,

$$\frac{\partial}{\partial t}(\rho \vec{V}) + \vec{\nabla} \cdot (\rho \vec{V} \otimes \vec{V}) = -\vec{\nabla} P + \vec{S}, \quad (3.14)$$

where \vec{S} denotes the external forces acting on the fluid. Alternately, this conservation relation may also be written:

$$\frac{\partial}{\partial t}(\rho \vec{V}) + (\rho \vec{V} \cdot \vec{\nabla}) \vec{V} = -\vec{\nabla} P + \vec{S}. \quad (3.15)$$

\vec{S} is here the sum of the Lorentz forces acting on both electrons and ions:

$$\begin{aligned} \vec{S} &= \vec{F}_i + \vec{F}_e \\ &= Z^* n_i (\vec{E} + \vec{V}_i \times \vec{B}) - e n_e (\vec{E} + \vec{V}_e \times \vec{B}) \\ &= e n_e (\vec{V}_i - \vec{V}_e) \times \vec{B}, \end{aligned} \quad (3.16)$$

where the last equality results from the electrical neutrality assumption $Z^* n_i = n_e$. Finally, introducing the current density $\vec{J} = e n_e (\vec{V}_i - \vec{V}_e)$:

$$\vec{S} = \vec{J} \times \vec{B}. \quad (3.17)$$

The energy conservation relation follows from the derivation of two equations expressing the balance of the kinetic energy and the internal energy components. The kinetic energy conservation equation reads [30]

$$\frac{\partial}{\partial t} \left(\frac{1}{2} \rho V^2 \right) + \vec{\nabla} \cdot \left[\left(\frac{1}{2} \rho V^2 \right) \vec{V} \right] = -\vec{\nabla} P \cdot \vec{V} + W, \quad (3.18)$$

W being the work produced by the Lorentz forces:

$$W = \vec{F}_i \cdot \vec{V}_i + \vec{F}_e \cdot \vec{V}_e = \vec{E} \cdot \vec{J}. \quad (3.19)$$

The derivation of a similar conservation relation for the internal energy [30] starts by writing the first law of thermodynamics,

$$dU = -Pd\Omega, \quad (3.20)$$

where U denotes the internal energy and Ω the volume. Introducing the mass internal energy $u = U/m_e$:

$$\frac{du}{dt} = \frac{P}{\rho^2} \frac{d\rho}{dt}. \quad (3.21)$$

Applying the relation

$$\frac{d}{dt} = \frac{\partial}{\partial t} + \vec{V} \cdot \vec{\nabla} \quad (3.22)$$

to both sides of this equation, and using the mass conservation Eq. (3.13) yields

$$\frac{\partial u}{\partial t} + \vec{V} \cdot \vec{\nabla} u = -\frac{P}{\rho} \vec{\nabla} \cdot \vec{V}. \quad (3.23)$$

The internal energy balance equation is obtained by summing the preceding equation multiplied by ρ and Eq. (3.13) multiplied by u :

$$\frac{\partial}{\partial t}(\rho u) + \vec{\nabla} \cdot (u \rho \vec{V}) = -P \vec{\nabla} \cdot \vec{V}. \quad (3.24)$$

Finally, one gets, adding Eq. (3.18) [also using Eqs. (3.19) and (3.24),

$$\frac{\partial}{\partial t} \left(\frac{1}{2} \rho V^2 + \rho u \right) + \vec{\nabla} \cdot \left[\left(\frac{1}{2} \rho V^2 + \rho h \right) \vec{V} \right] = \vec{E} \cdot \vec{J}, \quad (3.25)$$

h denoting the mass enthalpy $h = u + \frac{P}{\rho}$.

The Maxwell equations read

$$\frac{\partial \vec{B}}{\partial t} = -\vec{\nabla} \times \vec{E}, \quad (3.26)$$

$$\begin{aligned} \vec{\nabla} \times \vec{B} &= \mu_0 \vec{J}, \\ \vec{\nabla} \cdot \vec{B} &= 0, \\ \vec{\nabla} \cdot \vec{E} &= 0, \end{aligned} \quad (3.27)$$

with $\mu_0 = 4\pi \cdot 10^{-7}$ H/m denoting the magnetic permeability. The two first Eqs. (3.26) and (3.27) link electrical field \vec{E} , magnetic induction \vec{B} , and electric current density \vec{J} . Ohm's law provides the third relation necessary to obtain these quantities. Assuming that Hall effects can be neglected (this point will be verified later), Ohm's law reads

$$\vec{J} = \sigma(\vec{E} + \vec{V} \times \vec{B}). \quad (3.28)$$

Using Eq. (3.27):

$$\vec{J} \times \vec{B} = \frac{\vec{\nabla} \times \vec{B}}{\mu_0} \times \vec{B} = -\vec{\nabla} \left(\frac{B^2}{2\mu_0} \right) + \frac{(\vec{B} \cdot \vec{\nabla})\vec{B}}{\mu_0}. \quad (3.29)$$

The quantity on the right side of this equation is the divergence $\vec{\nabla} \cdot \vec{T}_{\text{em}}$ of the magnetic pressure tensor (also called the Maxwell tensor),

$$\vec{T}_{\text{em}} = -\frac{B^2}{2\mu_0} \vec{I} + \frac{\vec{B} \otimes \vec{B}}{\mu_0}, \quad (3.30)$$

whose elements read

$$T_{ij} = -\frac{B^2}{2\mu_0} \delta_{ij} + \frac{B_i B_j}{\mu_0}. \quad (3.31)$$

The momentum conservation Eq. (3.14) then reads

$$\begin{aligned} \frac{\partial}{\partial t}(\rho \vec{V}) + \vec{\nabla} \cdot (\rho \vec{V} \otimes \vec{V}) + \vec{\nabla} P \\ = -\vec{\nabla} \left(\frac{B^2}{2\mu_0} \right) + \frac{\vec{\nabla} \cdot (\vec{B} \otimes \vec{B})}{\mu_0}, \end{aligned} \quad (3.32)$$

or, alternately:

$$\begin{aligned} \frac{\partial}{\partial t}(\rho \vec{V}) + (\rho \vec{V} \cdot \vec{\nabla})\vec{V} + \vec{\nabla} P \\ = -\vec{\nabla} \left(\frac{B^2}{2\mu_0} \right) + \frac{(\vec{B} \cdot \vec{\nabla})\vec{B}}{\mu_0}. \end{aligned} \quad (3.33)$$

Let us here gather the equations that will be useful for our further developments:

$$\frac{\partial \rho}{\partial t} + \vec{\nabla} \cdot (\rho \vec{V}) = 0, \quad (3.34)$$

$$\frac{\partial}{\partial t}(\rho \vec{V}) + (\rho \vec{V} \cdot \vec{\nabla})\vec{V} + \vec{\nabla} P = -\vec{\nabla} \left(\frac{B^2}{2\mu_0} \right) + \frac{(\vec{B} \cdot \vec{\nabla})\vec{B}}{\mu_0}, \quad (3.35)$$

$$\frac{\partial}{\partial t} \left(\frac{1}{2} \rho V^2 + \rho u \right) + \vec{\nabla} \cdot \left[\left(\frac{1}{2} \rho V^2 + \rho h \right) \vec{V} \right] = \vec{E} \cdot \vec{J}, \quad (3.36)$$

$$\vec{J} = \sigma(\vec{E} + \vec{V} \times \vec{B}). \quad (3.37)$$

We will now consider the propagation of a planar shock in a cylindrical shock tube surrounded by a solenoid. The latter

induces a magnetic field \vec{B}_0 parallel to the cylindrical axis, which we will identify to the z axis. The upstream conditions will be denoted ρ_1, P_1 , and h_1 as concerns the density, the pressure, and the enthalpy, the gas velocity and the magnetic field being, respectively, $\vec{V}_1 = (0, 0, V_1)$ and $\vec{B}_1 = (0, 0, B_0)$. Their downstream counterparts will be $\rho_2, P_2, h_2, \vec{V}_2 = (0, 0, V_2)$ and $\vec{B}_2 = (0, 0, B_2)$. We will also assume low upstream electrical conductivity, i.e., $\sigma_1 \approx 0$, and the possibility of a strong increase of this quantity inside the shock front. Therefore, inside the shock, the gas velocity and magnetic field get components parallel to the shock plane and read $\vec{V} = (V_{\parallel}, 0, V_{\perp})$ and $\vec{B} = (B_{\parallel}, 0, B_{\perp})$, where the subscripts \perp and \parallel , respectively, denote the components perpendicular and parallel to the shock plane. The increase of the electrical conductivity induces an electric current \vec{J} in the shock plane, which in turn induces the parallel to the shock plane contribution to the magnetic field. The relation between B_{\parallel} and \vec{J} results from Maxwell-Ampère equation (3.27) and reads

$$\vec{J} = \left(0, \frac{1}{\mu_0} \frac{\partial B_{\parallel}}{\partial z}, 0 \right). \quad (3.38)$$

Finally, assuming that the shock plane remains normal to the z direction, all quantities involved in the problem are supposed to vary only with z coordinate, i.e., $\frac{\partial}{\partial x} \equiv 0$ and $\frac{\partial}{\partial y} \equiv 0$. We also consider stationary shock, i.e., $\frac{\partial}{\partial t} \equiv 0$.

Introducing the notation $[\mathcal{F}]_{z_0}^{z_0+\delta} = \mathcal{F}(z_0 + \delta) - \mathcal{F}(z_0)$, z_0 denoting the position of the upstream front and δ the shock thickness:

$$[\rho V]_{z_0}^{z_0+\delta} = 0, \quad (3.39)$$

$$[\rho V^2 + P]_{z_0}^{z_0+\delta} = \int_{z_0}^{z_0+\delta} \left[-\frac{\partial}{\partial z} \left(\frac{B^2}{2\mu_0} \right) + \frac{B_{\perp}}{\mu_0} \frac{\partial B_{\perp}}{\partial z} \right] dz, \quad (3.40)$$

$$\begin{aligned} \left[\left(\frac{1}{2} \rho V^2 + h \right) V \right]_{z_0}^{z_0+\delta} \\ = \int_{z_0}^{z_0+\delta} \left(\frac{1}{\mu_0} \frac{\partial B_{\parallel}}{\partial z} \right) \left[\frac{1}{\sigma \mu_0} \frac{\partial B_{\parallel}}{\partial z} - (V_{\parallel} B_{\perp} - V_{\perp} B_{\parallel}) \right] dz. \end{aligned} \quad (3.41)$$

Maxwell relation $\vec{\nabla} \cdot \vec{B} = 0$ yields $\frac{\partial B_{\perp}}{\partial z} = 0$, and the second of the above equations becomes

$$\left[\rho V^2 + P + \left(\frac{B_{\parallel}^2}{2\mu_0} \right) \right]_{z_0}^{z_0+\delta} = 0. \quad (3.42)$$

When the electrical conductivity σ inside the shock remains low, the above equations reduce to the usual Rankine-Hugoniot jump relations (3.2)–(3.4), applicable to shock propagation in absence of any magnetic field. Indeed, in that situation, no electric current can appear and, consequently, $\frac{\partial B_{\parallel}}{\partial z} = 0$. Shilkin *et al.* asserted that this is the case for their direct shock experiments on argon.

At the opposite, they claim that all of their reflected shocks are ionizing, and that electrical conductivities inside these shocks are then high enough to reach the conditions for “frozen-in” magnetic fields. Let us consider the extreme case

of infinite electrical conductivity σ . We then have then

$$\frac{1}{\sigma\mu_0} \frac{\partial B_{\parallel}}{\partial z} \ll -(V_{\parallel}B_{\perp} - V_{\perp}B_{\parallel}), \quad (3.43)$$

and also $B_{\parallel} \gg B_{\perp}$, yielding $V_{\parallel}B_{\perp} - V_{\perp}B_{\parallel} \approx -V_{\perp}B_{\parallel}$. The electric field inside the shock is $\vec{E} = -\vec{\nabla} \times \vec{B} \approx (0, -V_{\perp}B_{\parallel}, 0)$. Applying Maxwell relation $\vec{\nabla} \times \vec{E} = 0$, one obtains that $V_{\perp}B_{\parallel}$ is constant across the shock front. The jump relations in the limit $\sigma \rightarrow \infty$ then read

$$[\rho V]_{z_0}^{z_0+\delta} = 0, \quad (3.44)$$

$$[B_{\parallel} V]_{z_0}^{z_0+\delta} = 0, \quad (3.45)$$

$$\left[\rho V^2 + P + \left(\frac{B_{\parallel}^2}{2\mu_0} \right) \right]_{z_0}^{z_0+\delta} = 0, \quad (3.46)$$

$$\left[\left(\frac{1}{2} \rho V^2 + h + \frac{B_{\parallel}^2}{\mu_0} \right) V \right]_{z_0}^{z_0+\delta} = 0. \quad (3.47)$$

Since the gas velocities \vec{V} are taken at their upstream and downstream values (that are parallel to the z axis), V_{\perp} has been replaced by V in these equations. The two first relations can also be gathered to give

$$\left[\frac{B_{\parallel}}{\rho} \right]_{z_0}^{z_0+\delta} = 0. \quad (3.48)$$

The equality $[\rho V]_{z_0}^{z_0+\delta} = [B_{\parallel} V]_{z_0}^{z_0+\delta}$ is at the origin of the expression ‘‘frozen-in’’ magnetic field, since the evolution of B_{\parallel} follows exactly the one of the mass, as if magnetic lines are attached to matter.

σ is the key quantity that governs the evolution of the magnetic field inside the shock front. Using Eqs. (3.26)–(3.27), one gets the following induction equation:

$$\begin{aligned} \frac{\partial \vec{B}}{\partial t} &= -\vec{\nabla} \times \vec{E} = -\vec{\nabla} \times \left(\frac{\vec{J}}{\sigma} - \vec{V} \times \vec{B} \right) \\ &= -\frac{\vec{\nabla} \times (\vec{\nabla} \times \vec{B})}{\mu_0\sigma} + \vec{\nabla} \times (\vec{V} \times \vec{B}). \end{aligned} \quad (3.49)$$

The first term in the right member of the latter equation describes diffusion of the magnetic field, and the second term its advection by the fluid’s motion.

The magnetic Reynolds number, defined as the ratio

$$\mathcal{R}_m \equiv \frac{|\vec{\nabla} \times (\vec{V} \times \vec{B})|}{|\eta \vec{\nabla}^2 \vec{B}|}, \quad (3.50)$$

measures the relative importance of advection and diffusion of the magnetic field. The parameter $\eta = \frac{1}{\mu_0\sigma}$ (units: m^2/s) is the magnetic diffusivity. \mathcal{R}_m is of the order of

$$\mathcal{R}_m \approx \frac{VB/L_{\text{adv}}}{\eta/L_{\text{dif}}^2}, \quad (3.51)$$

where L_{adv} and L_{dif} are characteristic length scales for, respectively, advection and diffusion phenomena. In the absence of a shock wave perturbing the magnetized fluid, the two lengths may be considered equal, and the Reynolds number is given by the formula $\mathcal{R}_m = \mu_0\sigma VL$.

In the presence of a shock wave, the typical advection length is the thickness δ of the shock front, while the characteristic diffusion length is the dimension of the material through which the magnetic field passes, in the case of Shilkin’s experiments the diameter d of the cylinder containing the argon gas. We therefore write the Reynolds number in the context of shock experiments as

$$\mathcal{R}_m^* = \frac{VB/\delta}{\eta/d^2} = \mu_0\sigma V \frac{d^2}{\delta}. \quad (3.52)$$

From Shilkin *et al.*’s paper [7], we estimate typical velocity $V \approx 2.5$ km/s and note experimental electrical conductivities $1 (\Omega\text{m})^{-1} \lesssim \sigma \lesssim 10^3 (\Omega\text{m})^{-1}$, downstream incident shock wave, and $10^3 (\Omega\text{m})^{-1} \lesssim \sigma \lesssim 10^4 (\Omega\text{m})^{-1}$ behind the reflected shock wave. Experimentally, the shock thickness for argon at Mach numbers lying between 2 and 11 is in the range $3.7 \text{ mm} \lesssim \delta \lesssim 5.5 \text{ mm}$ [32–34]. Retaining $\delta = 5$ mm, and the diameter $d = 5$ cm of the cylindrical experimental device containing the argon gas, we get $0.16 \times 10^{-2} \lesssim \mathcal{R}_m^* \lesssim 0.16$ downstream the incident shock wave, and $0.16 \lesssim \mathcal{R}_m^* \lesssim 16$ behind the reflected one. These latter values are consistent with Shilkin *et al.*’s assertion that the magnetic field is frozen-in in their reflected shock experiments. We therefore introduce the magnetic pressures and mass internal energies in the Rankine-Hugoniot relations for the reflected shock. Noting, respectively, B and B_0 the magnetic induction downstream and upstream the reflected shock wave, they read [35–39]

$$\rho(D - V_H) = \rho_H D, \quad (3.53)$$

$$\rho(D - V_H)^2 + P + \frac{B^2}{2\mu_0} = \rho_H D^2 + \left(P_H + \frac{B_0^2}{2\mu_0} \right), \quad (3.54)$$

and

$$\frac{1}{2}(D - V_H)^2 + u + \frac{P}{\rho} + \frac{B^2}{\mu_0\rho} = \frac{1}{2}D^2 + u_H + \frac{P_H}{\rho_H} + \frac{B_0^2}{\mu_0\rho_H}. \quad (3.55)$$

The jump relation relative to the magnetic fields reads

$$\rho_0 B_H = \rho_H B_0. \quad (3.56)$$

D. Derivation of the resistivity tensor from the Boltzmann theory

In the presence of a magnetic field, Ohm’s law is no longer linear. The electric current and electric field are then related by the conductivity tensor $\bar{\sigma}$,

$$\vec{J} = \bar{\sigma} \vec{E} \Leftrightarrow \vec{E} = \bar{\eta} \vec{J}, \quad (3.57)$$

where we have introduced the resistivity tensor $\bar{\eta}$, i.e., the inverse of the conductivity tensor. The conductivity tensor derives from the Boltzmann transport theory, in terms of powers of the collision times. This will be the object of the first subsection. In the second one, we will discuss the possibility of calculating effective collisions times in the Ziman-Evans average-atom approach used in our paper.

The Boltzmann equation for electron transport reads [40]

$$\frac{\partial f_e}{\partial t} + \vec{v} \cdot \vec{\nabla} f_e - e(\vec{E} + \vec{v} \times \vec{B}) \cdot \frac{\partial f_e}{\partial \vec{p}} = I[f_e], \quad (3.58)$$

where f_e is the electron distribution function, \vec{v} the electron velocity, $\vec{p} = m_e \vec{v}$ the electron momentum, and $I[f_e]$ the collision integral. In the context of electric conduction, it is assumed that f_e is independent of time, and that it varies in space only through a possible temperature gradient, i.e., that

$$\frac{\partial f_e}{\partial \vec{r}} = \frac{\partial f}{\partial T} \frac{\partial T}{\partial \vec{r}}. \quad (3.59)$$

In the absence of such a gradient, the two first terms of the left-hand side of the Boltzmann equation can then be dropped. Another simplification consists of considering small perturbations around the Fermi-Dirac distribution function Eq. (2.2): $f_e = f(\epsilon, \mu) + \delta f$, with

$$\delta f = -\phi \frac{\partial f(\epsilon, \mu)}{\partial \epsilon}, \quad (3.60)$$

introducing a quantity ϕ depending on the configuration variables. Using the equality

$$\frac{\partial f}{\partial \vec{p}} = \vec{v} \frac{\partial f}{\partial \epsilon} \quad (3.61)$$

and only retaining the first order in ϕ , the Boltzmann equation then reduces to the following linearized form:

$$e\vec{v} \cdot \vec{E} \frac{\partial f}{\partial \epsilon} - e[\vec{v} \times \vec{B}] \frac{\partial f}{\partial \epsilon} \frac{\partial \phi}{\partial \vec{p}} = -\mathcal{L}[I], \quad (3.62)$$

$\mathcal{L}[I]$ denoting the linearized collision integral. Further writing [41]

$$\phi = \vec{p} \cdot \vec{\xi}(\epsilon), \quad (3.63)$$

the linearized collision term takes the following form, in terms of the collision time $\tau(\epsilon)$:

$$\mathcal{L}[I] = \vec{\xi} \cdot \vec{p} \frac{1}{\tau(\epsilon)}. \quad (3.64)$$

The linearized electron transport equation then reads [41]

$$e\vec{v} \cdot [\vec{E} + (\vec{\xi} \times \vec{B})] = -\vec{\xi} \cdot \vec{p} \frac{1}{\tau(\epsilon)}. \quad (3.65)$$

The most general decomposition of $\vec{\xi}$ is as follows:

$$\vec{\xi} = \alpha \hat{e} + \zeta \hat{b} + \gamma [\hat{e} \times \hat{b}], \quad (3.66)$$

with $\hat{b} = \vec{B}/B$ and $\hat{e} = \vec{E}/E$. Using this form in Eq. (3.65), one gets (we have dropped the energy dependence of $\tau(\epsilon)$ to lighten the formulas)

$$\alpha = -eE \frac{\tau}{m_e(1 + \omega_c^2 \tau^2)}, \quad (3.67)$$

$$\frac{\zeta}{\alpha} = (\omega_c \tau)^2 (\hat{e} \cdot \hat{b}), \quad (3.68)$$

and

$$\frac{\gamma}{\alpha} = -\omega_c \tau, \quad (3.69)$$

where $\omega_c = eB/m_e$ is the cyclotron frequency, and, finally [41],

$$\phi = -\frac{e\tau}{1 + (\omega_c \tau)^2} v_i [\delta_{ij} - \omega_c \tau \epsilon_{ijk} b_k + (\omega_c \tau)^2 b_i b_j] E_j. \quad (3.70)$$

The symbol ϵ_{ijk} represents the usual Levi-Civita one [42]:

$$\epsilon_{ijk} = \begin{cases} +1 & \text{if } (i, j, k) \text{ is } (1, 2, 3), (2, 3, 1), \text{ or } (3, 1, 2) \\ -1 & \text{if } (i, j, k) \text{ is } (3, 2, 1), (1, 3, 2), \text{ or } (2, 1, 3) \\ 0 & \text{if } i = j, \text{ or } j = k, \text{ or } k = i. \end{cases} \quad (3.71)$$

That is, ϵ_{ijk} is equal to 1 if (i, j, k) is an even permutation of $(1, 2, 3)$, to -1 if it is an odd permutation, and to 0 if any index is repeated. The cyclic permutations of $(1, 2, 3)$ are all even permutations, similarly the anticyclic permutations are all odd permutations. The derivation of the electric current vector \vec{J} follows immediately. Its components are

$$J_i = \frac{2}{(2\pi)^3} \int ev_i \delta f d^3k = \frac{2}{(2\pi)^3} \int ev_i \phi \frac{\partial f}{\partial \epsilon} d^3k. \quad (3.72)$$

Using Eq. (3.70),

$$J_i = \sigma_{ij} E_j, \quad (3.73)$$

where σ_{ij} are the components of the conductivity tensor that read

$$\sigma_{ij} = \delta_{ij} \sigma_0 - \epsilon_{ijm} b_m \sigma_1 + b_i b_j \sigma_2. \quad (3.74)$$

When the magnetic field is along the z direction,

$$\vec{\sigma} = \begin{pmatrix} \sigma_0 & -\sigma_1 & 0 \\ \sigma_1 & \sigma_0 & 0 \\ 0 & 0 & \sigma_0 + \sigma_2 \end{pmatrix}, \quad (3.75)$$

where

$$\sigma_n = \frac{4e^2}{3h^3 m_e} \int_0^\infty \frac{p^2}{2m_e} \frac{\tau(\omega_c \tau)^n}{1 + (\omega_c \tau)^2} \left(-\frac{\partial f}{\partial \epsilon} \right) 4\pi p^2 dp \quad (3.76)$$

or

$$\sigma_n = \frac{e^2}{3\pi^2 m_e} \int_0^\infty k^3 \frac{\tau(\omega_c \tau)^n}{1 + (\omega_c \tau)^2} \left(-\frac{\partial f}{\partial \epsilon} \right) d\epsilon. \quad (3.77)$$

The latter form can also be rewritten as

$$\sigma_n = \frac{e^2 n_e}{m_e} \left\langle \frac{\tau(\omega_c \tau)^n}{1 + (\omega_c \tau)^2} \right\rangle, \quad (3.78)$$

where

$$\left\langle \frac{\tau(\omega_c \tau)^n}{1 + (\omega_c \tau)^2} \right\rangle = \frac{1}{3\pi^2 n_e} \int_0^\infty k^3 \frac{\tau(\omega_c \tau)^n}{1 + (\omega_c \tau)^2} \left(-\frac{\partial f}{\partial \epsilon} \right) d\epsilon. \quad (3.79)$$

The resistivity tensor is the inverse of the conductivity one:

$$\vec{\eta} = \begin{pmatrix} \frac{\sigma_0}{\sigma_0^2 + \sigma_1^2} & \frac{\sigma_1}{\sigma_0^2 + \sigma_1^2} & 0 \\ -\frac{\sigma_1}{\sigma_0^2 + \sigma_1^2} & \frac{\sigma_0}{\sigma_0^2 + \sigma_1^2} & 0 \\ 0 & 0 & \frac{1}{\sigma_0 + \sigma_2} \end{pmatrix}. \quad (3.80)$$

E. Resistivity tensor at the limit $\omega_c \tau \ll 1$

One has, at order 2 in the expansion in $(\omega_c \tau)$,

$$\sigma_0 \approx \frac{e^2 n_e}{m_e} (\langle \tau \rangle - \omega_c^2 \langle \tau^3 \rangle) + O(\omega_c^3) \quad (3.81)$$

and

$$\sigma_1 \approx \frac{e^2 n_e}{m_e} \omega_c \langle \tau^2 \rangle + O(\omega_c^3),$$

which yields

$$\frac{\sigma_0}{\sigma_0^2 + \sigma_1^2} \approx \frac{m_e}{e^2 n_e} \frac{1}{\langle \tau \rangle} \left\{ 1 + \omega_c^2 \left(\frac{\langle \tau^3 \rangle}{\langle \tau \rangle} - \frac{\langle \tau^2 \rangle^2}{\langle \tau \rangle^2} \right) \right\} + O(\omega_c^3) \quad (3.82)$$

and

$$\begin{aligned} \frac{\sigma_1}{\sigma_0^2 + \sigma_1^2} &\approx \frac{m_e \omega_c}{e^2 n_e} \frac{\langle \tau^2 \rangle}{\langle \tau \rangle^2} \\ &\times \left\{ 1 + \omega_c^2 \left(2 \frac{\langle \tau^3 \rangle}{\langle \tau \rangle} - \frac{\langle \tau^2 \rangle^2}{\langle \tau \rangle^2} \right) \right\} + O(\omega_c^4). \end{aligned} \quad (3.83)$$

Noting that Eq. (2.1) can be rewritten,

$$\eta = \frac{m_e}{n_e e^2} \left\langle \frac{v}{\Lambda(\epsilon)} \right\rangle, \quad (3.84)$$

with

$$\left\langle \frac{v}{\Lambda(\epsilon)} \right\rangle = \frac{1}{3\pi^2 n_e} \int_0^\infty k^3 \frac{\partial f}{\partial \epsilon} \frac{v}{\Lambda(\epsilon)} d\epsilon, \quad (3.85)$$

where $\Lambda(\epsilon)$ is related to $\mathcal{I}(\epsilon)$ by

$$\frac{1}{\Lambda(\epsilon)} = \frac{\pi n_i}{k^4} \mathcal{I}(\epsilon), \quad (3.86)$$

one gets a collision time $\tau(\epsilon)$ from the data provided by our average-atom code:

$$\tau(\epsilon) = \frac{\Lambda(\epsilon)}{v}. \quad (3.87)$$

In the conditions of the experiments performed by Shilkin *et al.* on argon, we calculated this way values of the order of (in atomic units) $\langle \tau \rangle \approx 5 \times 10^2$, $\langle \tau^2 \rangle \approx 3 \times 10^5$ and $\langle \tau^3 \rangle \approx 3 \times 10^8$ for the shock velocity $D=2.5$ km/s. At the experimental magnetic induction $B = 5$ T, the cyclotron frequency is $\omega_c \approx 2 \times 10^{-5}$ a.u., which justifies the fact that the terms in ω_c^2 inside the brackets can be neglected. Finally, since

$$\frac{1}{\sigma_0 + \sigma_2} \approx \frac{m_e}{e^2 n_e} \frac{1}{\langle \tau \rangle} + O(\omega_c^5), \quad (3.88)$$

the resistivity tensor reads, in the conditions of Shilkin *et al.* experiments,

$$\bar{\eta} \approx \begin{pmatrix} \frac{1}{\sigma} & R_{\text{Hall}} B & 0 \\ -R_{\text{Hall}} B & \frac{1}{\sigma} & 0 \\ 0 & 0 & \frac{1}{\sigma} \end{pmatrix} + O(\omega_c^2), \quad (3.89)$$

where R_{Hall} denotes the Hall coefficient, given by

$$R_{\text{Hall}} = \frac{1}{en_e} \frac{\langle \tau^2 \rangle}{\langle \tau \rangle^2}. \quad (3.90)$$

In other words, the tension measured along the \hat{x} direction in these experiments gives the value of the electrical resistivity of the plasma unperturbed by a magnetic field, which then can be used for comparisons to calculations with the Ziman formula (2.1).

F. Hall coefficient using the average-atom approach

Using Eqs. (3.87) and (3.86) in Eq. (3.90) yields

$$R_{\text{Hall}} = \frac{1}{en_e} \times 3\pi^2 n_e \frac{\int_0^\infty k^3 \left(-\frac{\partial f}{\partial \epsilon}\right) \left(\frac{\Lambda}{v}\right)^2 d\epsilon}{\left[\int_0^\infty k^3 \left(-\frac{\partial f}{\partial \epsilon}\right) \left(\frac{\Lambda}{v}\right) d\epsilon\right]^2}. \quad (3.91)$$

The dimensionless Hall constant r_{Hall} is obtained by multiplying R_{Hall} by en_e , i.e., $r_{\text{Hall}} = R_{\text{Hall}} \times en_e$.

At both solid state and nondegenerate plasma limits, the formula recovers the expected $r_{\text{Hall}} = 1$ value. In the former case,

$$\lim_{T \rightarrow 0} \left(-\frac{\partial f}{\partial \epsilon} \right) = \delta(\epsilon - \epsilon_F), \quad (3.92)$$

yielding, using the equality $k_F^3 = 3\pi^2 n_e$:

$$\lim_{T \rightarrow 0} r_{\text{Hall}} = (3\pi^2 n_e) \frac{k_F^3 \tau^2(\epsilon_F)}{k_F^6 \tau^2(\epsilon_F)} = 1. \quad (3.93)$$

The plasma electron degeneracy parameter is defined as the ratio of thermal energy on Fermi energy:

$$\Theta = \frac{k_B T}{\epsilon_F} = \frac{2m_e}{\hbar^2} \frac{k_B T}{(3\pi^2 n_e)^{2/3}}. \quad (3.94)$$

In the nondegenerate plasma limit $\Theta \gg 1$:

$$-\frac{\partial f}{\partial \epsilon} \rightarrow \beta e^{-\beta(\epsilon - \mu)}. \quad (3.95)$$

$\beta e^{-\beta(\epsilon - \mu)} \ll 1$ and is a decreasing function of ϵ . Expanding the scattering phase shifts $\delta_\kappa(k)$ and the ion-ion structure factor $S(k)$ in powers of k , and only retaining the first terms

$$\delta_\kappa(k) \propto k \text{ and } S(k) \propto k, \quad (3.96)$$

$I(\epsilon)$ varies as k^3 and $\Lambda(\epsilon) \propto k$. Then $\tau(\epsilon) \approx C + O(k)$, C denoting a constant, and, at the lowest order in the expansion,

$$\lim_{\Theta \gg 1} r_{\text{Hall}} = (3\pi^2 n_e) \frac{\int_0^\infty k^3 \left(-\frac{\partial f}{\partial \epsilon}\right) C^2 d\epsilon}{\left[\int_0^\infty k^3 \left(-\frac{\partial f}{\partial \epsilon}\right) C d\epsilon\right]^2} = 1, \quad (3.97)$$

using the equality $\int_0^\infty k^3 \left(-\frac{\partial f}{\partial \epsilon}\right) d\epsilon = 3\pi^2 n_e$.

The value $r_{\text{Hall}} = 1$ is also predicted in the strong magnetic fields ($\omega_c \tau \gg 1$). Indeed, at order 4 in the expansions in $1/(\omega_c \tau)$,

$$\sigma_0 \approx \frac{e^2 n_e}{m_e} \frac{1}{\omega_c^2} \left(\left\langle \frac{1}{\tau} \right\rangle - \frac{1}{\omega_c^2} \left\langle \frac{1}{\tau^3} \right\rangle \right), \quad (3.98)$$

$$\sigma_1 \approx \frac{e^2 n_e}{m_e} \frac{1}{\omega_c} \left(1 - \frac{1}{\omega_c^2} \left\langle \frac{1}{\tau^2} \right\rangle \right), \quad (3.99)$$

which yield, only retaining the most important term when calculating the ratio $\frac{\sigma_1}{\sigma_0^2 + \sigma_1^2}$:

$$\lim_{\omega_c \tau \gg 1} r_{\text{Hall}} = 1 - \frac{1}{\omega_c^2} \left(\left\langle \frac{1}{\tau} \right\rangle^2 - \left\langle \frac{1}{\tau^2} \right\rangle \right). \quad (3.100)$$

IV. ELECTRICAL CONDUCTIVITY AND HALL RESISTIVITY OF SHOCKED ARGON: CALCULATIONS

A. Description of our plasma equation-of-state model

The solution of the Rankine-Hugoniot relations requires the knowledge of the equation of state. Estimations of the

TABLE I. Parameters entering the OCP plasma model for the ionic contribution to the equation of state [see Eq. (4.4)].

k	a_k	b_k
1	-0.895929	4.666486
2	0.11340656	13.675411
3	-0.90972827	1.8905603
4	-0.11614773	1.0277554

downstream temperature T_H request $U(\rho, T)$ and $P(\rho, T)$. To this end, we build an equation-of-state model for argon according to the decomposition:

$$U(\rho, T) = U_c(\rho) + U_{i,\text{th}}(\rho, T) + U_{e,\text{th}}(\rho, T)$$

$$P(\rho, T) = P_c(\rho) + P_{i,\text{th}}(\rho, T) + P_{e,\text{th}}(\rho, T). \quad (4.1)$$

$U_c(\rho)$ and $P_c(\rho)$ denote the 0 K isotherms, also named cold curves. $U_{e,\text{th}}(\rho, T)$ and $P_{e,\text{th}}(\rho, T)$ are the electronic thermal contributions, obtained by removing the $T = 0$ K electronic energies and pressures from the total electronic ones:

$$\begin{cases} U_{e,\text{th}}(\rho, T) &= U_e(\rho, T) - U_e(\rho, 0) \\ P_{e,\text{th}}(\rho, T) &= P_e(\rho, T) - P_e(\rho, 0). \end{cases} \quad (4.2)$$

$U_e(\rho, T)$ and $P_e(\rho, T)$ are calculated with our average-atom code PARADISIO. The cold contributions $U_c(\rho)$ and $P_c(\rho)$ are the ones of the SESAME equation of state SESAME 5172 of argon [43,44]. SESAME 5172 incorporates the physics of six theoretical models. It provides very good agreement with experimental shock data in the very low density range (initial density: $\rho_0 = 1.34 \times 10^{-3}$ g/cm³) [43,45], thereby justifying our choice of these cold contributions. A more recent SESAME 5173 model [44] was developed to improve agreement with high-pressure Hugoniot (above 90 GPa) as well as with low-temperature data for fluid and solid argon, including phase boundaries, i.e., in areas outside the scope of our paper. Finally, the one-component plasma (OCP) model [46] is used for the thermal ionic contributions,

$$\begin{cases} U_{i,\text{th}}(\rho, T) &= \rho k_B T + \frac{\rho}{3} \Delta U_i(\rho, T) \\ P_{i,\text{th}}(\rho, T) &= \frac{2}{3} \rho k_B T + \Delta U_i(\rho, T), \end{cases} \quad (4.3)$$

where

$$\frac{\Delta U_i(\rho, T)}{k_B T} = \min \left(\left[\Gamma^{3/2} \sum_{k=1}^4 \frac{a_k}{(b_k + \Gamma)^{k/2}} - a_1 \Gamma \right], \frac{3}{2} \right), \quad (4.4)$$

Γ being the usual ionic coupling parameter:

$$\Gamma = \frac{Z^*2}{(k_B T) R_{\text{ws}}}. \quad (4.5)$$

The values of the parameters a_k and b_k are given in Table I:

B. Thermodynamic conditions reached in the shock experiments of Shilkin *et al.*

Table II gives the thermodynamic conditions ρ_H , T_H , and P_H obtained from solving the Rankine-Hugoniot relations, and using our EOS model for argon, for each experimental shock velocities D provided by Shilkin *et al.* Before the initial

TABLE II. First part of the table: Principal Hugoniot. The initial matter velocity is $V_0 = 0$. Second part: After the reflected shock wave, assuming frozen-in magnetic field lines. The initial matter velocities V_0 are the velocities V_H reached on the principal Hugoniot. Since the shock is totally reflected on the obstacle, the downstream mass velocity is the opposite of V_0 and therefore $V_H - V_0 = 0$.

$D - V_0$ (km/s)	ρ_H (g/cm ³)	T_H (K)	P_H (GPa)	$V_H - V_0$ (km/s)
Principal Hugoniot ($V_0 = 0$)				
2.53	2.457×10^{-2}	5199	2.945×10^{-2}	1.912
2.56	2.461×10^{-2}	5315	3.016×10^{-2}	1.936
2.63	2.468×10^{-2}	5541	3.153×10^{-2}	1.980
2.85	2.500×10^{-2}	6498	3.748×10^{-2}	2.166
2.91	2.510×10^{-2}	6757	3.915×10^{-2}	2.216
2.97	2.523×10^{-2}	7000	4.077×10^{-2}	2.264
3.20	2.588×10^{-2}	7944	4.763×10^{-2}	2.458
3.27	2.613×10^{-2}	8223	4.985×10^{-2}	2.519
3.40	2.664×10^{-2}	8737	5.418×10^{-2}	2.634
3.51	2.712×10^{-2}	9159	5.802×10^{-2}	2.734
Behind the reflected shock wave, with $B = 5$ T (V_0 : previous V_H values)				
2.53	6.357×10^{-2}	10423	1.600×10^{-1}	0
2.56	6.413×10^{-2}	10564	1.638×10^{-1}	0
2.63	6.537×10^{-2}	10897	1.728×10^{-1}	0
2.85	6.945×10^{-2}	11875	2.027×10^{-1}	0
2.91	7.063×10^{-2}	12141	2.115×10^{-1}	0
2.97	7.191×10^{-2}	12407	2.210×10^{-1}	0
3.20	7.753×10^{-2}	13429	2.624×10^{-1}	0
3.27	7.942×10^{-2}	13740	2.762×10^{-1}	0

shocks, argon is assumed to be at ambient temperature $T_0 = 300$ K and at pressure $P_0 = 0.4$ MPa [7]. According to our EOS, these conditions imply that the initial argon gas density is $\rho_0 = 6 \times 10^{-3}$ g/cm³.

Figures 4–6 display, respectively, the density, temperature and pressure as functions of the shock velocity in the

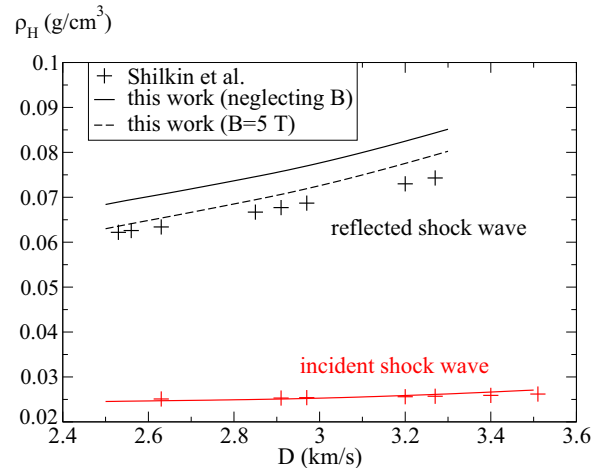


FIG. 4. Density versus shock velocity on the principal (incident shock wave) and secondary (reflected shock wave) Hugoniot curves. Comparison between our results without magnetic field, with a magnetic field $B = 5$ T, and the experiments of Shilkin *et al.* [7].

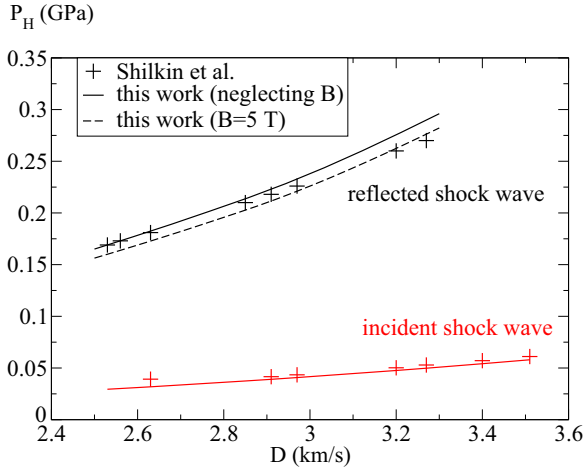


FIG. 5. Pressure versus shock velocity on the principal (incident shock wave) and secondary (reflected shock wave) Hugoniot curves. Comparison between our results without magnetic field, with a magnetic field $B = 5$ T, and the experimental values [7].

conditions of the shock experiments of Shilkin *et al.* [7]. The crosses represent experimental values: in red for the initial shocks and in black for the reflected ones. The lines, with the same color code, correspond to our calculations of the conditions reached in these experiments. For the reflected shocks, we present two results: one obtained when the magnetic field is absent in the Rankine-Hugoniot equations (black full line) and the other when taking into account the field $B = 5$ T (black dashes). The former case supposes that the reflected shocks do not ionize the argon plasma enough to ensure frozen-in magnetic lines, whereas the latter considers that ionization is strong enough to fully get this effect. Our results assuming the frozen-in applied $B = 5$ T magnetic field present the closest agreement with the experimental densities and pressures. The agreement is particularly improved concerning the densities (see Fig. 4). The temperature reached

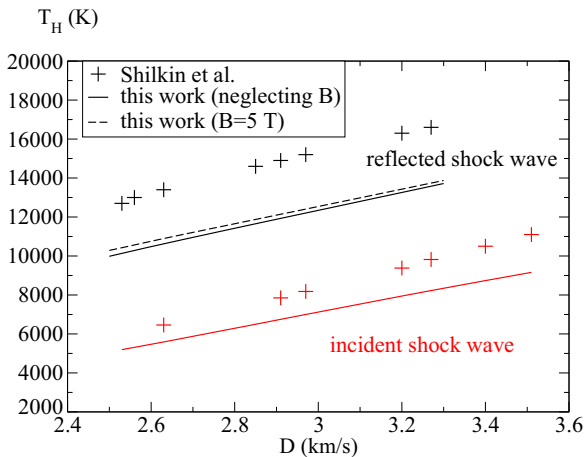


FIG. 6. Temperature versus shock velocity on the principal (incident shock wave) and secondary (reflected shock wave) Hugoniot curves. Comparison between our results without magnetic field, with a magnetic field $B = 5$ T, and the calculated values of Shilkin *et al.* [7].

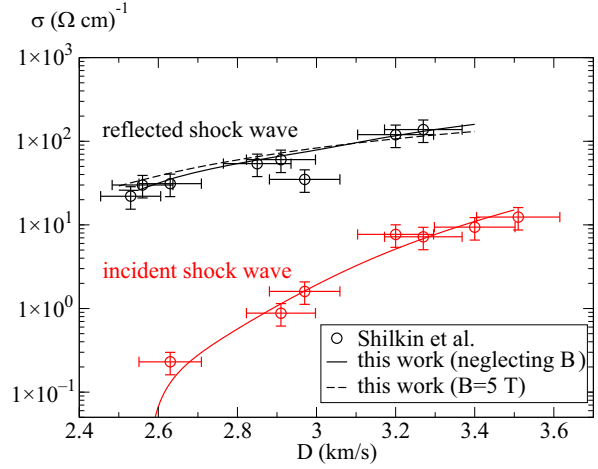


FIG. 7. Electrical conductivity versus shock velocity on the principal (incident shock wave) and secondary (reflected shock wave) Hugoniot curves. Comparison between our results without magnetic field, with a magnetic field $B = 5$ T, and the experiments of Shilkin *et al.* [7].

downstream the shock waves was not measured by Shilkin *et al.* The values (crosses) presented in Fig. 6 are theoretical and noticeably higher than our own theoretical values. These discrepancies are due to different equation-of-state models, the temperature being particularly sensitive to them.

C. Electrical conductivity and Hall coefficient of shocked argon: Comparison between experiment and theory

Figure 7 represents conductivity calculations of argon for incident and reflected shock waves compared to the measurements by Shilkin *et al.* The calculated conductivities are the inverse of the resistivities obtained with Eq. (2.1), using the phase shifts and mean ionic charges given by the average-atom code PARADISIO for argon at the densities ρ_H and temperatures T_H given in Table II. The color code is the same as in Figs. 4–6. We observe global good agreement with experimental values, both for the incident and reflected shock waves. For the latter ones, we present results obtained when the magnetic field is taken into account or not in the shock equations. They differ only slightly, despite fairly different upstream densities (see Fig. 4).

Hall effect in plasmas has been investigated using transport-equation theories, mainly in the nondegenerate limit. These approaches consider interaction between individual species composing the plasma, while our average-atom one describes electrons interacting with others and with mean ions through a mean field. The most accurate models include electron-electron and electron-neutral atom collisions in addition to electron-ion ones. Table III gives the Hall constant values obtained in the nondegenerate limit according to the collision terms taken into account by the transport-equation models, and compares them with our mean-atom result. More details on these models are given in the following text.

The electrical and thermal conduction of fully ionized plasma, (i.e., a plasma formed of electrons and ions, with no neutral atoms) has been studied by Spitzer and Härn in

TABLE III. We compare our calculated Hall constant value to the ones obtained with transport-equation approaches in the case of non-degenerate electrons. The crosses indicate the collision terms taken into account in different models. Our average-atom (AA) result is close to the Braginskii and the LRT (linear response theory) number 2 ones accounting for direct electron-electron interactions, as well as to the LRT 3 one that also includes electron-neutral atom collisions.

Model	NONDEGENERATE LIMIT			r_{Hall}
	$e-i$	$e-e$	$e-n$	
Braginskii [48]	×	×		1.207
Lee and More [49]	×			1.9328
Stygar <i>et al.</i> [50]	×			1.9328
LRT 1 [11,13]	×			1.933
LRT 2 [11,13]	×	×		1.199
LRT 3 [11]	×	×	×	$\simeq 1.5$
Our paper ($\Theta = 1000$)	mean collision time (AA and T matrix)			1.25

the classical low density limit within kinetic theory [47]. The linearized Fokker-Planck kinetic equation is solved with a Landau collision integral including both electron-ion ($e-i$) and electron-electron ($e-e$) collisions.

Braginskii introduced the magnetic field in this approach, extending it to the Hall effect [48]. An expression has been established for the Hall resistivity $\eta_{\text{Hall}} = R_{\text{Hall}}B$ in terms of powers of $(\omega_c \tau)$:

$$\eta_{\text{Hall}} = \frac{B}{en_e} + \frac{m_e}{e^2 n_e \tau} \left[\frac{(\omega_c \tau)(\alpha_0'' + \alpha_1''(\omega_c \tau)^2)}{\delta_0 + \delta_1(\omega_c \tau)^2 + (\omega_c \tau)^4} \right]. \quad (4.6)$$

At the limit $\omega_c \tau \ll 1$, the Braginskii Hall constant r_{Hall} reads

$$r_{\text{Hall}} = en_e \times R_{\text{Hall}} = 1 + \frac{\alpha_0''}{\delta_0}. \quad (4.7)$$

The Lorentz plasma is a plasma with highly ionized ions, no neutral atoms, and in which electron-electron collisions can be neglected. For that plasma, Braginskii calculates $\alpha_0'' = 0.094$ and $\delta_0 = 0.0961$, yielding $r_{\text{Hall}}^{Z \gg 1} = 1.978$. When the atoms are only once ionized: $\alpha_0'' = 0.7796$, $\delta_0 = 3.7703$, and $r_{\text{Hall}}^{Z=1} = 1.207$.

Braginskii as well as Spitzer-Härm theories are rigorously valid only for fully ionized, (i.e., all atoms are at least ionized one) nondegenerate plasmas.

Lee and More's model of transport properties [49] takes into account the electron degeneracy by using the Fermi-Dirac distribution function for the electrons. Boltzmann's equation is solved within the relaxation-time approximation (RTA). Electrical and thermal conductivity, thermoelectric power, and also Hall, Nernst, Ettinghausen, and Leduc-Righi coefficients, essential to the study of plasmas in presence of electromagnetic fields, are considered. The transport properties are expressed in computationally simple forms and apply to any electron degeneracy. In the completely nondegenerate limit ($\mu\beta \rightarrow -\infty$), the Hall constant value is $r_{\text{Hall}}^{LM} = 1.9328$, and is close to Braginskii's one for the Lorentz plasma, which assumes that all atoms are strongly ionized. The standard

$r_{\text{Hall}} = 1$ value for solids is recovered in the totally degenerate limit $\mu\beta \rightarrow \infty$.

Stygar *et al.* [50] developed a quantum-mechanical approach for the electrical conductivity tensor for a Lorentz plasma in a weak magnetic field within the linearized Boltzmann transport approach. Stygar *et al.* evaluated the Coulomb logarithms in the second Born approximation. They read

$$\ln \Lambda(v_e) = \left(\ln \chi - \frac{1}{2} \right) + \left[\left(\frac{2Z^* e^2}{\lambda m_e v_e^2} \right) (\ln \chi - \ln 2^{4/3}) \right], \quad (4.8)$$

with $\chi = 2m_e v_e \lambda / \hbar$, $\lambda = \max(\lambda_D, R_{\text{ws}})$, λ_D being the Debye length, given by

$$\lambda_D = \left[\left(\frac{4\pi n_e e^2}{k_B T} \right) + \left(\frac{4\pi Z^* n_e e^2}{k_B T} \right) \right]^{-1/2}. \quad (4.9)$$

v_e denotes the electron velocity. Finally, Stygar *et al.* obtained the following expression for the Hall constant:

$$r_{\text{Hall}}^{SGF} = \frac{315\pi}{512} \left(\frac{\ln \Lambda(v_{e1})}{\ln \Lambda(v_{e2})} \right)^2, \quad (4.10)$$

with

$$v_{e1} = \left(\frac{7k_B T}{m_e} \right)^{1/2},$$

$$v_{e2} = \left(\frac{10k_B T}{m_e} \right)^{1/2}. \quad (4.11)$$

$\frac{315\pi}{512} \approx 1.9328$, i.e., Lee and More's value for r_{Hall} in the nondegenerate limit. Predicted values of the Hall constant applying Lee and More's model and Stygar *et al.*'s are, respectively, represented in Fig. 9 by the black dashes and the black line.

The plasma ionization downstream the shock waves generated in argon in the experiments of Shilkin *et al.* is far too weak for the application of Lee and More as well as Stygar *et al.*'s models, which both assume Lorentz plasmas. These models and, more generally, any RTA approach, do not recover Spitzer and Härm's result for electrical conductivity in the nondegenerate limit. This is attributed to the fact that $e-e$ collisions, not taken into account in the RTA, grow in importance when the atoms are less ionized and that they can then no more be neglected. Interpolation procedures have been proposed to correct the RTA electrical conductivities [50,51], but there is no equivalent for correcting RTA Hall constants.

Adams *et al.* used an approach based on LRT within the Zubarev formalism [8,9] that allows for a systematic treatment of $e-e$ collisions at any degeneracy [13]. LRT is a quantum statistical approach based on the grand canonical ensemble, linearized with respect to nonequilibrium perturbations such as external fields [9,52,53]. LRT takes into account all interactions, including $e-e$ ones, through equilibrium force-force correlation functions. Electron-neutral-atom ($e-n$) collisions are also taken into account. Transport coefficients are calculated using a converging expansion in terms of so-called generalized moments. When $e-e$ collisions are neglected in the theory, Adams *et al.* recovered the $r_{\text{Hall}} = 1.9328$ RTA value in the nondegenerate limit, and obtained $r_{\text{Hall}} = 1.1994$

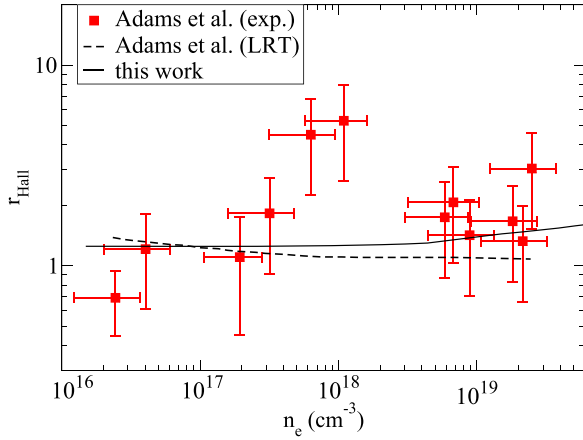


FIG. 8. $r_{\text{Hall}} = R_{\text{Hall}} \times en_e$ as a function of electron density n_e . Red squares and black dashes: The experimental and theoretical (using LRT) values of Adams *et al.* [11]. Black full line: Our results.

when e - e collisions are accounted for. The latter value is very close to the one $r_{\text{Hall}}^{Z=1} = 1.207$ calculated by Braginskii for atoms ionized once. When e - n collisions are taken into account, the Hall constant is enhanced up to $r_{\text{Hall}} \approx 1.5$ for the less degenerate argon plasmas, according to Ref. [11]. Since that work, the authors presented in Ref. [13] an extension of LRT to include the effects of an external magnetic field, which results in a value only slightly higher than the standard $r_{\text{Hall}} = 1$ Hall constant.

Figure 8 compares our calculated r_{Hall} constants (black line) with the experimental ones (red squares) deduced by measured Hall voltages by Shilkin *et al.* Hall voltage is proportional to R_{Hall} , and the experimental r_{Hall} are obtained using theoretical electron densities n_e from SAHA IV code. The figure also presents the theoretical values obtained by Adams *et al.* using the linear response theory approach [53]. Our Ziman average-atom approach takes into account interactions between mean ions and electrons, and the interactions between electrons through their total charge density and through the exchange-correlation potential. At high degeneracy parameters Θ , we calculate values for the Hall constant r_{Hall} close to Adams *et al.*'s LRT and Braginskii's one for a low density plasma composed of ions with the lowest possible charge $Z = 1$, no neutral atoms and electrons, where the e - e collisions between are considered (see Fig. 9, where the arrow points on that value).

As electron degeneracy increases, (i.e., as Θ decreases), Adams *et al.* predicted, within the LRT approach, the decrease of r_{Hall} in shocked argon in Shilkin *et al.* experiments as shown by the black dashes in Fig. 8 (the degeneracy parameter Θ varies inversely to n_e). At the opposite, we obtain increased r_{Hall} values as electron degeneracy rises, getting closer to the RTA values, which are considered as becoming more relevant as degeneracy is stronger. Oppositely, at the highest electron density obtained in the experiments, for which we estimate degeneracy parameters of the order of 15, Adams *et al.* calculated r_{Hall} values, decreasing with Θ , and becoming very close to the standard $r_{\text{Hall}} = 1$ value expected for highly degenerate plasmas ($\Theta \ll 1$) and for solids.

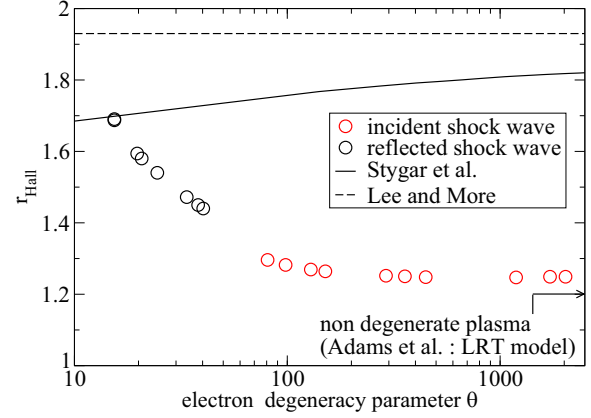


FIG. 9. r_{Hall} versus electron degeneracy parameter Θ . Red circles: Our results, in conditions reached downstream the principal shock waves. Black circles: Our results, behind the reflected shocks. Black dashes: Lee and More model [49]. Black line: Stygar *et al.* model. The arrow points to the value predicted by Adams *et al.* in the totally nondegenerate limit when electron-electron collisions are taken into account in collision integrals for the fully ionized $Z = 1$ plasma [13].

As in the nondegenerate case, we summarize, in Table IV, the results obtained with transport-equation methods according to the included collision terms, in the case of the partially degenerate argon plasma ($\Theta = 20$), and compare them to our average-atom result.

In next section, we are going to take a closer look at our comparisons with the LRT calculations of Adams *et al.*

V. DISCUSSION: AVERAGE-ATOM VERSUS LRT APPROACHES FOR THE HALL CONSTANT

For solids, as well as for low density hot plasmas, the Hall constant has the so-called standard value $r_{\text{Hall}} = 1$. Our calculated values in the conditions of the experiments of Shilkin *et al.* are significantly different from the ones obtained by

TABLE IV. We compare our calculated Hall constant value to the ones obtained with transport equation approaches in the case of partial electron degeneracy parameter $\Theta = 20$. Our result is close to the ones of Lee and More and of Stygar *et al.*, which are becoming more relevant since electron exchange-correlation effects are becoming increasingly important compared with e - e direct collisions. In the text, we suggest a possible explanation for the fact that the LRT is already tending towards the expected $r_{\text{Hall}} = 1$ value for the fully degenerate case.

PARTIAL ELECTRON DEGENERACY $\Theta = 20$				
Model	Included collision terms			Hall constant r_{Hall}
	e - i	e - e	e - n	
Lee and More [49]	×			1.93
Stygar <i>et al.</i> [50]	×			1.69
LRT [11,13]	×	×	×	$\simeq 1$
Our paper	mean collision time (AA and T-matrix)			1.69

Adams *et al.* [10–13] using LRT approach within Zubarev’s method, which raises questions.

The LRT approach takes into account electron-ion, electron-neutral, and electron-electron collisions, enabling for a complete description of partially ionized plasmas, for which the value of r_{Hall} is unknown. One limitation to its use could be the difficulty to build cross sections for the scattering of electrons by neutral atoms. Because of the lack of theoretical electron-atom cross sections for argon at the date of their work, Adams *et al.* [11,13] used experimental data, obtained for argon at ambient temperature. The method used for the calculation of the plasma composition (density of neutrals, ions and electrons) also introduces some uncertainty. In the case of the largest argon densities in the experiments of Shilkin *et al.*, Adams *et al.* reported as much as 40% differences in the theoretical electron densities obtained according to whether the SAHA IV code of Gryaznov [54] or the COMPTRA program [55] is used for that purpose [11] (both codes are based on similar chemical pictures for the plasma equations of state, but use different thermodynamical models).

The average-atom approach used in the present paper presents its own difficulties. First, the separation between bound and free electrons may be problematic [19,28]. However, this does not concern argon in the density and temperature ranges reached in the experiments of Shilkin *et al.* The bound-free separation is unambiguous, and all possible definitions for the mean ion charge Z^* [19] converge to the same value. The question remains of properly accounting for e - n and e - e interactions with average-atom methods.

Let us start looking at the way that average-atom methods handle the scattering of electrons by neutral atoms. In the experiments of Shilkin *et al.*, kinetic models considered that argon plasmas are composed, outside the electrons, of neutral and ionized argon atoms, and use two distinct approaches, on the one hand for the e - n collision times and on the other for all e - i ones. The average-atom approach used in the present paper avoids the problem of distinguishing ions and neutral atoms, which are replaced by identical ions with the same mean charge Z^* . In the considered experiments, the neutral atoms are about 10^2 up to 10^6 times more numerous than ionized argon atoms. Thus, the mean ion is almost a neutral argon atom, and the average-atom model actually provides an e - n collision time that extrapolates the average-atom e - i collisions time to the limit $Z^* \rightarrow 0$. Posterior to Adams *et al.*’s works, Quan *et al.* derived e - n and e - i model potentials with the aim to build theoretical e - n and e - i scattering cross sections [56]. For e - n scattering, the model potential reads

$$V(r) = V_s(r) + V_p(r) + V_x(r), \quad (5.1)$$

where $V_s(r)$ is the sum of the electron-nucleus Coulomb potential and of the free electron-bound electrons Coulomb interactions, $V_x(r)$ an exchange potential, and $V_p(r)$ a polarization potential. The e - i model potential only differs from the e - n one by a screening factor e^{-r/r_D} , $r_D = \sqrt{k_B T / 4\pi n_e}$ being the Debye screening length, which applies to the Coulomb term $V_s(r)$. Quan *et al.*’s e - i model potential tends then to the e - n one in the limit $Z^* \rightarrow 0$ (since $n_e \rightarrow 0$), and the e - n scattering cross section appears as the $Z^* \rightarrow 0$ limit of the e - i one, as in the average-atom approach.

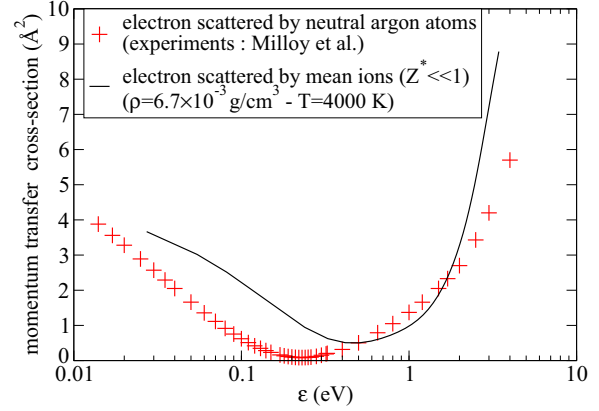


FIG. 10. Momentum transfer cross section for electron- neutral argon collisions. Red crosses: Experiments of Milloy *et al.* [57]. Black line: The average-atom code is used to calculate the cross section for an electron scattered by an almost neutral argon atom (case of argon at density $\rho = 6.7 \times 10^{-3}$ g/cm³ and temperature $T = 4000$ K, for which $Z^* < 10^{-5}$).

The average-atom effective potential includes the same two Coulomb contributions and electron exchange potential too. Polarizability does not appear explicitly, but is, in some way, present through electron exchange and correlations. The problem is whether this is sufficient to reproduce the experimental cross sections, given that the polarization potential makes a significant contribution to the model of Quan *et al.* [56]. Unfortunately, we were not able to calculate the cross section for the scattering of electrons by almost neutral atoms for argon at ambient temperature with our average-atom code. We only obtained converged results for somewhat higher densities and temperatures. Figure 10 compares the average-atom momentum transfer cross section for electron collisions with almost neutral atoms obtained for $\rho = 6.7 \times 10^{-3}$ g/cm³ and $T = 4000$ K (represented by the black line) to the experimental cross section for electron-neutral atom collisions measured for argon at ambient temperature by Milloy *et al.* (red crosses). Qualitatively, the average-atom calculation is in fairly good agreement with the experiments. In particular, a Ramsauer-Townsend-like minimum is also predicted with the average-atom approach, albeit at a somewhat higher collision energy than experimentally. One must also keep in mind that the actual plasma temperatures are about 10^4 K in the experiments. For this reason, we think that our average-atom approach, which allows for electron density and temperature changes, is relevant for e - n interactions, despite the fact that the neutral atoms are approximated by ions carrying low charges Z^* .

To explain any discrepancies with other theoretical approaches, like the LRT one, the possibility remains that the average-atom models do not properly take into account the e - e interactions. The inclusion of e - e direct collisions in density functional theory (DFT) approaches for transport properties is the subject of discussions in the literature. In a paper published in 2006 [58], Dharma-wardana advanced strong arguments in favor of DFT-based approaches for e - e interactions. Indeed, he pointed out that the electron current is conserved under e - e interactions, since the electron current operator commutes fully with the e - e interaction Hamiltonian,

and that this holds at any electron degeneracy. The e - e interactions only contribute indirectly to the resistivity through the e - i effective potential. Dharma-wardana developed these arguments further in a very recent article (see Sec. II in the Supplemental Material of Ref. [59]). The counterargument put forward against DFT-based approaches is that the latter consider the electrons as an aggregate, through their total charge density, rather than as individuals interacting with each other as is done in kinetic theories such as the Boltzmann equation [53,60]. It is, however, expected that both DFT-based methods and kinetic approaches will converge as electron degeneracy grows, resulting from the increasing compensation of e - e interactions by the exchange-correlation potential.

The nondegenerate limit $\Theta \rightarrow \infty$ is the most largely studied by kinetic methods, mainly for totally ionized plasmas in which all ions are at least ionized once. Braginskii's value $r_{\text{Hall}} = 1.207$ when all atoms are ionized once is confirmed by Adams *et al.*'s LRT value $r_{\text{Hall}} = 1.199$ obtained assuming the same plasma composition. Both approaches include e - e direct interactions. When the latter are neglected, $r_{\text{Hall}} = 1.9328$ [49,50], which is clearly higher. In the electron degeneracy range $100 \lesssim \Theta \lesssim 2 \times 10^3$, corresponding to Shilkin *et al.*'s experiments in incident shocks, in which the mean ion charge Z^* remains small, our average-atom approach yields the value $r_{\text{Hall}} \approx 1.25$, close to the one expected when e - e interactions are properly taken into account. This result backs up the arguments put forward in the literature in favor of the suitability of DFT-based methods for the study of transport properties.

But, accounting within LRT for scattering of electrons by neutral atoms besides a low concentration of atoms ionized once, Adams *et al.* obtained very different results, presented in two articles, Refs. [11,12]. In both works, e - n scattering times were derived from the experimental scattering cross sections measured at ambient temperature presented in Fig. 10. In the second paper, the LRT was extended to explicitly include the magnetic field, which was not the case in the first one. Within the extended LRT, the $B = 5$ T field applied by Shilkin *et al.* was found to reduce the theoretical r_{Hall} value (see Fig. 4 in Ref. [12]), whereas, using the nonmodified LRT approach, the value is raised up to $r_{\text{Hall}} \approx 1.5$ in the less degenerate cases. In the modified LRT approach, transport coefficients are written as ratios of polynomials in $X = (\omega_c \tau_0)^2$, where τ_0 is given by the one-moment LRT mean scattering time. The authors observed that, for weakly coupled plasmas, even magnetic fields below $B = 5$ T impact the values of transport coefficients (including electrical, thermal conductivities, as well as Hall constant).

As electron degeneracy grows, (i.e., as Θ diminishes), we observed, within our average-atom approach, a strong dependency of the Hall constant r_{Hall} on the electron density and the temperature. This is clearly not predicted by Adams *et al.*, which found that the Hall constant value tends rapidly towards $r_{\text{Hall}} = 1$, as expected for degenerate plasmas, whether or not the standard or extended LRT model was used. A possible source for the observed discrepancy between LRT results and ours is the use, within LRT, of an experimental ambient temperature scattering cross section for e - n scattering while the temperatures exceed 10^4 K. Indeed, it can easily be shown that, using the same cross section regardless of the increase of temperature, r_{Hall} decreases as the T grows.

Using the following relation between the cross-section Q_{en} for scattering of electrons by neutral atoms and the collision time τ_{en} ,

$$\hbar k n_n Q_{\text{en}}(\epsilon) = \frac{1}{\tau_{\text{en}}(\epsilon)}, \quad (5.2)$$

yields, at temperature T_0 :

$$r_{\text{Hall}}^0 = (3\pi^2 n_e) \times \frac{\int_0^\infty \frac{k^3}{(kQ_{\text{en}})^2} \left(-\frac{\partial f}{\partial \epsilon}\right)_0 d\epsilon}{\left[\int_0^\infty \frac{k^3}{(kQ_{\text{en}})^2} \left(-\frac{\partial f}{\partial \epsilon}\right)_0 d\epsilon\right]^2}. \quad (5.3)$$

In the temperature and density conditions considered in this paper: $\left(-\frac{\partial f}{\partial \epsilon}\right)_0 \approx \beta_0 e^{-\beta_0(\epsilon - \mu_0)}$. Let us increase the temperature by a small quantity $\delta T \ll T_0$. At first order of the expansion in $\delta T/T_0$, the resulting variation in the derivative of the Fermi-Dirac distribution function reads

$$\begin{aligned} \left(-\frac{\partial f}{\partial \epsilon}\right) &\approx \left(-\frac{\partial f}{\partial \epsilon}\right)_0 e^{\beta_0 \frac{\delta T}{T_0} (\epsilon - \mu_0)} \\ &\approx \left(-\frac{\partial f}{\partial \epsilon}\right)_0 \left(1 + \beta_0 \frac{\delta T}{T_0} (\epsilon - \mu_0)\right), \end{aligned} \quad (5.4)$$

and the Hall constant at $T = T_0 + \delta T$ is

$$r_{\text{Hall}} \approx r_{\text{Hall}}^0 \left\{ 1 + \frac{\delta T}{T_0} \left[1 + \beta_0 \frac{\int_0^\infty \frac{k^3(\epsilon - \mu_0)}{(kQ_{\text{en}})^2} \left(-\frac{\partial f}{\partial \epsilon}\right)_0 d\epsilon}{\int_0^\infty \frac{k^3}{(kQ_{\text{en}})^2} \left(-\frac{\partial f}{\partial \epsilon}\right)_0 d\epsilon} - 2\beta_0 \frac{\int_0^\infty \frac{k^3(\epsilon - \mu_0)}{(kQ_{\text{en}})^2} \left(-\frac{\partial f}{\partial \epsilon}\right)_0 d\epsilon}{\int_0^\infty \frac{k^3}{(kQ_{\text{en}})^2} \left(-\frac{\partial f}{\partial \epsilon}\right)_0 d\epsilon} \right] \right\}. \quad (5.5)$$

In the thermodynamical conditions reached in the experiments of Shilkin *et al.*, the chemical potential has a large negative value $-9 \lesssim \mu_0 \lesssim -4.5$ (atomic units), and only the lowest energies ϵ contribute to the integrals. Therefore, taking $(\epsilon - \mu_0) \approx -\mu_0$, the previous equation is simplified to

$$r_{\text{Hall}} \approx r_{\text{Hall}}^0 \left(1 + \frac{\delta T}{T_0} [1 - \beta_0 \mu_0]\right), \quad (5.6)$$

and, finally, using the relation, valid for electron degeneracy parameters $\Theta > 1$,

$$e^{\beta_0 \mu_0} = \frac{4}{3\sqrt{\pi}} \Theta_0^{-3/2}, \quad (5.7)$$

one gets, after having replaced $\ln[4/(3\sqrt{\pi})]$ by its numerical value:

$$\frac{\delta r_{\text{Hall}}}{r_{\text{Hall}}^0} \approx -\frac{\delta T}{T_0} \left(0.285 + \frac{3}{2} \ln \Theta_0\right). \quad (5.8)$$

Therefore, if one uses the same experimental cross section for the scattering of electrons by neutral atoms regardless of temperature changes, the calculated Hall constant decreases when temperature grows.

VI. CONCLUSION

We presented calculations of the resistivity of shocked argon within Ziman formalism combined with the relativistic quantum average-atom method. We have compared our results with measurements performed in experiments involving both incident and reflected shock waves in the presence of a

magnetic field of 5 Tesla. Beyond the experimental electric conductivities, the other important objective of these experiments was to measure the Hall resistivity, in view of deducing the experimental electron density, or, equivalently, the mean ionic charge.

The average-atom code PARADISIO was used for the calculation of the equation of state for argon, as well as for the scattering phase shifts needed for the scattering amplitude of electrons by the mean ions, and for the mean ion charge Z^* . We took into account the magnetic field in the Rankine-Hugoniot relations and derived, starting from the Boltzmann equation, the resistivity tensor in terms of the mean electron-ion collision time $\tau(\epsilon) = \Lambda(\epsilon)/v$ (see Sec. III E), i.e., the inverse of the collision frequency used in the Ziman resistivity formula.

It turns out that the effect of a 5 Tesla magnetic field on the calculation of electrical conductivity is rather limited in the conditions of the experiments. This also justifies the small magnetic field assumption $\omega_c \tau \ll 1$ made for the derivation of the resistivity tensor $\bar{\eta}$. The off-diagonal element η_{12} giving the Hall resistivity then reads $R_{\text{Hall}} B = r_{\text{Hall}} B / (en_e)$, where the dimensionless Hall constant r_{Hall} is the ratio $r_{\text{Hall}} = \frac{\langle \tau^2 \rangle}{\langle \tau \rangle^2}$.

We presented Hall constant r_{Hall} calculations based on the use of the average-atom code PARADISIO for the relaxation time $\tau(\epsilon)$, in the conditions reached in the shock experiments of Shilkin *et al.* carried out on argon. In our approach, $\tau(\epsilon) = \Lambda(\epsilon)/v$ is the inverse of the mean electron-ion collision frequency used for the Ziman resistivity calculation. We compared our results to experimental values derived from the Hall voltage measurements by Shilkin *et al.*, as well as to theoretical ones from Adams *et al.*, based on the quantum statistical linear-relaxation-time approach within the Zubarev formalism.

Both sets of results are in the (large) experimental error bars, but within our approach, r_{Hall} values rise with electron densities and are closer to the central experimental values. Our results are in good agreement with Adams *et al.*'s in the case of the less degenerate plasmas, for which the relevance of DFT-based models is nevertheless questionable. A growing discrepancy with Adams *et al.* appears as both electron density and temperature rise, which we explain by the fact that Adams *et al.* used an ambient temperature experimental scattering cross section for electron scattering by neutral atoms when the actual temperatures exceed 10^4 K.

-
- [1] S. Atreya, P. Mahaffy, H. Niemann, M. Wong, and T. Owen, *Planet. Space Sci.* **51**, 105 (2003).
- [2] F. Hersant, D. Gautier, and J. I. Lunine, *Planet. Space Sci.* **52**, 623 (2004).
- [3] O. Mousis, J. I. Lunine, J.-M. Petit, S. Picaud, B. Schmitt, D. Marquer, J. Horner, and C. Thomas, *Astrophys. J.* **714**, 1418 (2010).
- [4] A. Kramida, Yu. Ralchenko, J. Reader, and NIST ASD Team, NIST Atomic Spectra Database (ver. 5.11), National Institute of Standards and Technology, Gaithersburg, MD, <https://physics.nist.gov/asd> (accessed April 23, 2024).
- [5] I. V. Ivanov, V. B. Mintsev, V. E. Fortov, and A. N. Dremin, *Zh. Eksp. Teor. Fiz.* **71**, 216 (1976).
- [6] L. Gatilov, V. Glukhodedov, F. Grigor'ev, S. Korner, L. Kuleshova, and M. Mochalev, *J. Appl. Mech. Tech. Phys.* **26**, 88 (1985).
- [7] N. S. Shilkin, S. V. Dudin, and V. K. Gryaznov, *Sov. Phys.-JETP* **97**, 922 (2003).
- [8] D. N. Zubarev, V. G. Morozov, and G. Röpke, *Statistical Mechanics of Nonequilibrium Processes, (See 3527400834): Basic Concepts, Kinetic Theory* (Wiley-VCH, Weinheim, Germany, 1996), Vol. 1.
- [9] G. Röpke, *Nonequilibrium Statistical Physics* (John Wiley & Sons, New York, 2013).
- [10] J. R. Adams, H. Reinholz, R. Redmer, V. B. Mintsev, N. S. Shilkin, and V. K. Gryaznov, *Phys. Rev. E* **76**, 036405 (2007).
- [11] J. R. Adams, H. Reinholz, R. Redmer, N. S. Shilkin, V. B. Mintsev, and V. K. Gryaznov, *Contrib. Plasma Phys.* **47**, 331 (2007).
- [12] J. R. Adams, N. S. Shilkin, V. E. Fortov, V. K. Gryaznov, V. B. Mintsev, R. Redmer, H. Reinholz, and G. Röpke, *Phys. Plasmas* **14**, 062303 (2007).
- [13] J. R. Adams, H. Reinholz, and R. Redmer, *Phys. Rev. E* **81**, 036409 (2010).
- [14] S. B. Hansen, W. A. Isaacs, P. A. Sterne, B. G. Wilson, V. Sonnad, and D. A. Young, Electrical conductivity calculations from the Purgatorio code, Technical Report No. UCRL-PROC-218150 (Lawrence Livermore National Lab. (LLNL), Livermore, CA, 2006).
- [15] P. A. Sterne, S. B. Hansen, B. G. Wilson, and W. A. Isaacs, *High Energy Density Phys.* **3**, 278 (2007).
- [16] G. Faussurier and C. Blancard, *Phys. Rev. E* **100**, 033202 (2019).
- [17] M. W. C. Dharma-wardana, D. D. Klug, L. Harbour, and L. J. Lewis, *Phys. Rev. E* **96**, 053206 (2017).
- [18] N. Wetta and J.-C. Pain, *Phys. Rev. E* **102**, 053209 (2020).
- [19] N. Wetta and J.-C. Pain, *Phys. Rev. E* **108**, 015205 (2023).
- [20] H. Minoo, C. Deutsch, and J. Hansen, *Phys. Rev. A* **14**, 840 (1976).
- [21] J. M. Ziman, *Philos. Mag.* **6**, 1013 (1961).
- [22] R. Evans, B. L. Gyroffy, N. Szabo, and J. M. Ziman, The properties of liquid metals, in *Proceedings of the Second International Conference on Tokyo 1972* (Taylor and Francis, London, UK, 1973), pp. 319–331.
- [23] M. Pénicaud, *J. Phys.: Condens. Matter* **21**, 095409 (2009).
- [24] D. A. Liberman, *Phys. Rev. B* **20**, 4981 (1979).
- [25] V. V. Karasiev, T. Sjostrom, J. Dufty, and S. B. Trickey, *Phys. Rev. Lett.* **112**, 076403 (2014).
- [26] S. Groth, T. Dornheim, and M. Bonitz, *Contrib. Plasma Phys.* **57**, 137 (2017).
- [27] M. Abramowitz, I. A. Stegun, and D. Miller, *J. Appl. Mech.* **32**, 239 (1965).
- [28] N. Wetta and J.-C. Pain, *Contrib. Plasma Phys.* **62**, e202200003 (2022).
- [29] F. Rogers, *J. Chem. Phys.* **73**, 6272 (1980).

- [30] L. Landau and E. Lifshitz, *Fluid Mechanics* (Pergamon Press, Oxford, UK, 1987), Vol. 6.
- [31] L. Euler, Mémoires de l'académie des sciences de Berlin **11**, 274 (1757).
- [32] H. Alsmeyer, *J. Fluid Mech.* **74**, 497 (1976).
- [33] F. Robben and L. Talbot, *Phys. Fluids* **9**, 633 (1966).
- [34] B. Schmidt, *J. Fluid Mech.* **39**, 361 (1969).
- [35] F. De Hoffmann and E. Teller, *Phys. Rev.* **80**, 692 (1950).
- [36] H. L. Helfer, *Astrophys. J.* **117**, 177 (1953).
- [37] C. F. Kennel, *AIP Conf. Proc.* **314**, 180 (1994).
- [38] R. Mallick, *Phys. Rev. C* **84**, 065805 (2011).
- [39] R. P. H. Berton, *CEAS Space J.* **13**, 83 (2021).
- [40] W. Ebeling, V. E. Fortov, Y. L. Klimontovich, N. P. Kowalenko, W. D. Kraeft, Y. E. Krasny, D. Kremp, P. Kulik, and V. A. Riabii, *Transport Properties of Dense Plasmas* (Akademie-Verlag, Berlin, 1984).
- [41] A. Harutyunyan and A. Sedrakian, *Phys. Rev. C* **94**, 025805 (2016).
- [42] J. R. Tyllesley, *An Introduction to Tensor Analysis: For Engineers and Applied Scientists* (Longman, New York, 1973).
- [43] J. H. Carpenter, S. Root, K. R. Cochrane, D. G. Flicker, and T. K. R. Mattsson, Equation of state of argon: Experiments on Z, density functional theory (DFT) simulations, and wide-range model, Technical Report No. SAND2012-7991 (Sandia National Laboratories (SNL), Albuquerque, NM, and Livermore, CA, 2012).
- [44] S. Root, C. A. McCoy, K. R. Cochrane, J. H. Carpenter, R. W. Lemke, L. Shulenburg, T. R. Mattsson, and P. A. Sterne, *Phys. Rev. B* **106**, 174114 (2022).
- [45] D. B. Garcia, D. M. Dattelbaum, P. M. Goodwin, S. A. Sheffield, J. S. Morris, R. L. Gustavsen, and M. W. Burkett, *AIP Conf. Proc.* **1793**, 050012 (2017).
- [46] J. P. Hansen, *Phys. Rev. A* **8**, 3096 (1973).
- [47] L. Spitzer, Jr. and R. Härm, *Phys. Rev.* **89**, 977 (1953).
- [48] S. Braginskii, *Rev. Plasma Phys.* **1**, 205 (1965).
- [49] Y. T. Lee and R. More, *Phys. Fluids* **27**, 1273 (1984).
- [50] W. A. Stygar, G. A. Gerdin, and D. L. Fehl, *Phys. Rev. E* **66**, 046417 (2002).
- [51] V. Fortov, V. Ternovoi, M. Zhernokletov, M. A. Mochalov, A. L. Mikhailov, A. S. Filimonov, A. A. Pyalling, V. B. Mintsev, V. K. Gryaznov, and I. L. Iosilevskii, *Sov. Phys.-JETP* **97**, 259 (2003).
- [52] G. Röpke, *Phys. Rev. A* **38**, 3001 (1988).
- [53] H. Reinholz, G. Röpke, S. Rosmej, and R. Redmer, *Phys. Rev. E* **91**, 043105 (2015).
- [54] V. Gryaznov, I. Iosilevskii, and V. Fortov, *Zh. Prikl. Mekhan. i Tekhn. Fiz.* **3**, 70 (1973).
- [55] S. Kuhlbrodt, B. Holst, and R. Redmer, *Contrib. Plasma Phys.* **45**, 73 (2005).
- [56] W. Quan, X. Sun, and Q. Chen, *Phys. Plasmas* **27**, 112701 (2020).
- [57] H. Milloy, R. Crompton, J. Rees, and A. Robertson, *Aust. J. Phys.* **30**, 61 (1977).
- [58] M. W. C. Dharma-wardana, *Phys. Rev. E* **73**, 036401 (2006).
- [59] M. W. C. Dharma-wardana, [arXiv:2404.19692](https://arxiv.org/abs/2404.19692).
- [60] M. P. Desjarlais, C. R. Scullard, L. X. Benedict, H. D. Whitley, and R. Redmer, *Phys. Rev. E* **95**, 033203 (2017).